Flexural, Compressive, and Tensile Properties of Pultruded GFRP Bars

by

Mahmoud Abou Niaj

Bachelor of Science in Civil Engineering, Beirut Arab University, 2016

A Report Submitted in Partial Fulfillment
of the Requirements for the Degree of

Master of Engineering

in the Graduate Academic Unit of Civil Engineering

Supervisors: Alan Lloyd, PhD, Civil Engineering
Gobinda Saha, PhD, P.Eng, Mechanical Engineering

Examining Board: Kaveh Arjomandi, PhD, P.Eng, Civil Engineering
Xiomara Sanchez-Castillo, PhD, P.Eng, Civil Engineering

This report is accepted by the
Dean of Graduate Studies

THE UNIVERSITY OF NEW BRUNSWICK

December, 2018

ABSTRACT

Glass fibre reinforced polymer (GFRP) bars are an attractive alternative for steel reinforcement to resist the tensile stresses generated in reinforced concrete members because of their high tensile strength and strong resistance against corrosion. However, unlike steel, GFRP is a brittle material that cause brittle member behavior when used in structural components. To ensure safe and efficient use of the material, it is important to test GFRP in different loading scenarios to fully understand its material properties. In this study, pultruded GFRP bars were tested in flexure and tension according to ASTM standards, whereas in compression, a new testing method was proposed as there is still no standard test method made yet specific for testing GFRP bars in compression. The data obtained from all tests performed were used in a sectional analysis to check horizontal equilibrium in the section, and compare between the moment resistance and the applied moment.

DEDICATION

Dedicated to my beloved family

ACKNOWLEDGEMENTS

I would like to express my sincere gratitude and appreciation to my supervisors Dr. Alan Lloyd and Dr. Gobinda Saha for their help and guidance throughout the whole length of the degree and especially in this project. I would like also to thank every professor at the University of New Brunswick from whom I took a course. These courses were captivating and enriched with valuable theoretical and practical knowledge that I will apply in my professional career.

Table of Contents

List of Tables

List of Figures

1. Introduction

1.1 Background Information

Steel reinforcement bars have traditionally been the best option for reinforcement in concrete members to resist tensile stresses and partially resist shear stresses generated from the loads applied on them. However, due to the chemical composition of steel and the corrosive environmental conditions reinforced concrete (RC) members may be subjected to, steel corrosion can be a problem that cause a reduction in the strength of those members which could lead to failure. This issue raised the interest in finding an alternative for steel reinforcement. Glass fibre reinforced polymer (GFRP) bars became an alluring alternative because of the advantages that GFRP has over steel.

The major advantage that GFRP has over steel is its ability to resist corrosion, which allow structures built in severe corrosive environmental conditions stay safe and durable. Furthermore, GFRP has many other properties that makes it a very appropriate alternative to substitute steel ([1] and [2]), which include the following:

- Light weight that can be approximated as ¼ of that of steel bars.
- High tensile strength that can reach approximately double that of steel bars.
- Insulating properties against heat and electricity.
- Dimensional flexibility, where it can be manufactured in different shapes and sizes.
- Low lifecycle costs.
- Coefficient of expansion similar to that of concrete which helps in avoiding the cracks, and the internal stresses generated in the concrete structure due to temperature changes.

1.2 Objectives

The purpose of this project is to determine the mechanical properties of pultruded GFRP bars. The GFRP bars tested in this study had a diameter of 9.25 mm and were tested in flexure, compression, and tension. Digital image correlation (DIC) was used to monitor the response of the specimens during testing. The tested bars were manufactured at the labs of the University of New Brunswick using existing machines that can produce bars with diameters of 9.25 mm.

The objectives of this work are summarized in the following:

1. Mechanically test the bars using standard test methods in tension and flexure, and check to which extent these methods are applicable and if they need to be improved.
2. Find a new method to test GFRP bars in compression.
3. Determine the material properties in all loading scenarios including: type of failure, ultimate strength, and elastic modulus.
4. Check equilibrium in the section, and how the moment resistance can be compared to the applied moment.
5. Find an alternative method to determine the mechanical properties of the bars without having the need to perform all three tests.

1.3 Digital Image Correlation (DIC)

Digital image correlation is an optical 3-D, full-field, and non-contact measuring technique that can measure, with high level of accuracy, deformations and strains on almost every type of material using a relatively inexpensive digital cameras [3]. Figure 1 shows the two cameras used in DIC measurements mounted on a tripod with attached lights.

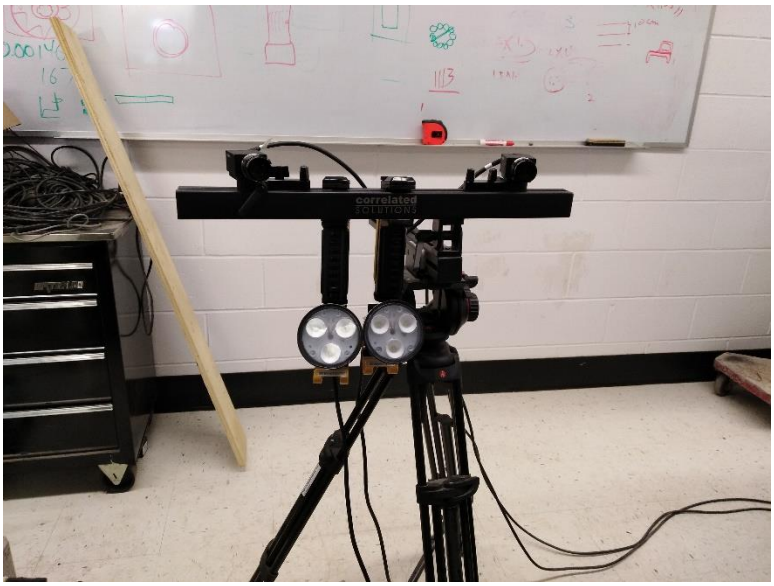

Figure 1- DIC cameras used

The concept of DIC for measuring displacements and strains is based on the principle of cross correlation between images, where it compares a reference image that is un-deformed to a series of deformed images. The reference image is divided in to a grid of small squares called subsets that has recognizable patterns in each one of them, and then the software searches in a specific search zone of a deformed image for a subset that has the most similarity to the subset's patterns in the reference image. The difference between the target subset and the reference subset is the measured displacement. To obtain measurements with high level of accuracy, each subset needs to be sufficiently unique compared to the

surrounding subsets in the search zone, and achieving this uniqueness depends on the image texture of the tested material. So, to achieve optimal uniqueness for each subset, the image texture needs to be improved. That can be obtained by creating an artificial pattern, also known as speckle pattern, on the measured specimen which can be achieved by spraying the specimen with white paint so that it becomes completely white, and then spraying it with black paint to create a randomly sized and shaped patterns that are distinct from each other. These patterns deform along the measured surface and improve the cross correlation between the images [4]. After calculating the displacements, DIC computes the strains from the displacement data by dividing the change in distance between the speckles inside the subsets ($\Delta L = L_t - L_0$) over the original distance between them (L_0).

Figure 2 [4] shows the measuring technique DIC uses to compute displacements.

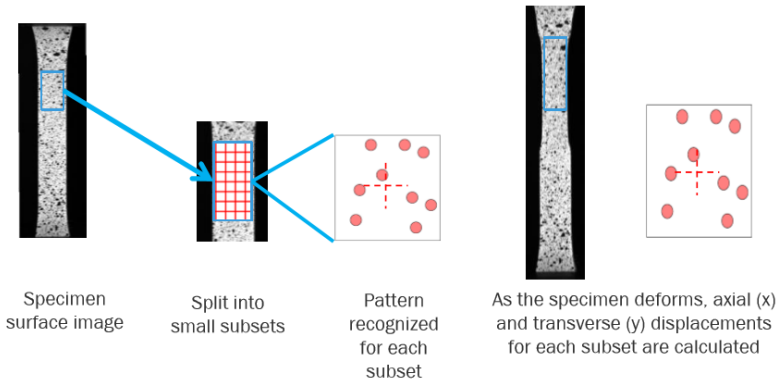

Figure 2- Digital image correlation measurement technique [4]

2. Literature Review

The increase in the demand for GFRP as reinforcing bars attracted the attention of many researchers. These researchers have performed testing on bars to determine their mechanical properties in tension, compression, and flexure and examine the bars' behavior in these loading scenarios, in order to use them more properly and design members that are reinforced with such type of material with higher level of reliability. In this chapter, several research papers that contain information about GFRP bars testing are reviewed.

Khan et al. [5] tested 15.9 mm pultruded GFRP bars in both tension and compression using ASTM standard test methods, ASTM D7205/7205M-06 [13] for the former test and a modified version of ASTM D695-15 [12] for the latter test. In tension, they tested three bars each having a length of 1555 mm and had their anchorage lengths coated by sand, they used anchors that had a length of 460 mm, with inner and outer diameters of 30 mm and 45 mm respectively. The anchors were filled with expansive cement which was allowed 72 hours curing to reach its maximum expansive pressure. The bars were tested using a loading rate between 1 and 1.3 mm/min. They tested five 80 mm GFRP bars in compression by modifying ASTM D695-15 [12], where, they replaced the hardened blocks with two high strength steel plates to make the specimens perfectly aligned with the loading machine and test them with a similar loading rate they used in the tension test. The elastic modulus obtained in both tension and compression was 56 GPa and 42 GPa respectively, and the average ultimate strength in both tension and compression was 1395 MPa and 846 MPa respectively. The failure modes obtained were characterized in the splitting of the free length fibres in tension, and the crushing of fibres and not their buckling in compression.

Figure 3(a) and Figure 3(b) below show the tensile and compressive failure modes obtained in the tension and compression tests performed by Khan et al. [5] respectively.

(a) (b)

Figure 3- (a) Failure mode in tension (b) Failure mode in compression [5]

Khorramian et al. [6] considered modifying ASTM D695-15 [12] test standard in a way to make it able to test GFRP bars in compression (like many other researchers do including Khan et al. [5]) to be unacceptable, as it is designed to test rigid plastics in compression and not GFRP. For that purpose they proposed a new test method to test GFRP bars in compression, where, they limited the length of the tested specimen to be twice the bar diameter. The test method they proposed was concerned the most about the gripping mechanism on the bar to avoid premature failure and ensure perfect alignment with the testing machine which will ensure the concentricity of the load applied. Adhesive anchors and steel caps were used to confine the bar and ensure perfect alignment with the load to ensure premature failure did not occur and full compressive capacity was achieved at the

end of the test. The compressive elastic modulus obtained from this testing method was different than what ASTM D695-15 [12] would give, where, it gave a compressive elastic modulus of 49.3 GPa which is larger than what Khan [5] obtained using ASTM D695-15 [12] by 17 %. The failure mode obtained was similar to what Khan [5] obtained in his compression test which was the crushing of the fibres and not their buckling. Figure 4 below shows the failure mode obtained from the compression test done by Khorramian et al. [6].

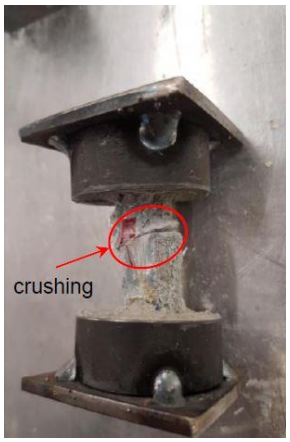

Figure 4- Failure mode in compression [6]

Benmokrane et al. [7] tested four different types of FRP bars in tension using a similar test setup to ASTM D7205/7205M-06 [13] which Khan [5] used in his experiments. The tested specimens they used had a length of 1600 mm and were embedded in a 600 mm steel anchors that had an inner diameter of 30 mm that was grouted with high performance resin grout. At the end of the test they were able to achieve failure in the free length indicating that the test can be used to determine the ultimate tensile strength of the bars.

Kocaoz et al. [8] used the same approach that Khan [5] and Benmokrane [7] used to test the bars in tension with the addition of threading the bars in the anchorage lengths to try increase the friction between the bar and the cementitious material in the anchors. They tested four types of GFRP bars that had a diameter of 12.5 mm and free length between anchors of 500 mm, 40 times the bar diameter. The anchorage lengths were embedded inside steel pipes that were grouted with an expansive cementitious material, and the bars were threaded 200 mm from their ends with 2 threads per cm. The controlling failure mode observed at the end of the test is the splitting in the free length fibres, and the mean tensile strength obtained was 990 Mpa which, when compared to what Khan [5] obtained using ASTM D7205/7205M-06 [13], was smaller by 29%.

Castro et al. [9] experimented on GFRP bars in tension where he tested bars having a diameter of 9 mm to determine their tensile properties. Similary to what Khan et al. [5], Benmokrane et al. [7], and Kocaoz et al. [8] had done, he used metal anchors to embed the bars' anchorage lengths in. The anchors had a diameter of 23.4 mm and wall thickness of 1.1 mm, and the anchorage length was computed as 15 times the bar diameter. However, Castro[9] used a different cementitious material to what other researchers used in their experiments where he used a high strength gypsum cement mixed with washed and dried concrete sand passing through sieve #20 (850 μm) to increase the shear friction of the cementitious material. Similar to the previously mentioned studies, failure occurred in the free length of the bar, and the tensile elastic modulus obtained was 37.405 GPa which is less than that obtained by Khan et al. [5] by 33%.

Bowlby et al. [10] tested 9.2 mm GFRP bars in Flexure and Tension according to ASTM D790 [11] and ASTM D3916 [14] respectively. The flexure test performed was a 3-point bending test, and the tensile test performed used steel pipes that had an outer diameter of 25.4 mm and an inner diameter of 20 mm as anchors to grip the bar from each end in order to attach it properly to the testing machine. Expansive mortar known as Rockfrac that has a curing pressure that can reach 138 MPa was poured inside the steel pipes to keep them firmly attached to the bar to help the test carry on until failure occurs. However, failure didn't occur and the bar slipped during testing preventing it reaching failure. They suggested to sand coat the anchorage lengths of the bars before pouring the expansive mortar in the anchors to increase the shear friction between the mortar and the bar to avoid the slipping of the bar.

3. Testing Methodology

Three different tests were done on the GFRP bars which are: Flexure test, Compression test, and Tension test. ASTM (American Society for Testing and Materials) testing standards were adopted for both flexural and tensile tests, which are ASTM D7205/7205M-06 [13] and ASTM-D790 - 17 [11] respectively. However, for testing GFRP bars in compression, a new testing method had to be introduced since there is no specific standard test method developed yet to determine the mechanical properties of GFRP bars in compression.

3.1 Flexure Test

ASTM D790–17 [11] "*Standard Test Methods for Flexural Properties of Unreinforced and Reinforced Plastics an Electrical Insulating Materials*" is used widely to determine the flexural properties of GFRP bars through a 3-point bending test.

3.1.1 Tested Specimens Number and Dimensions

Five GFRP bars, in accordance with ASTM D790 – 17 [11] specifications, were tested. Each bar was the same material with a diameter of 9.25 mm. The test standard specifies that the supported length of the bar should have a depth to length ratio of 1:16, so according to this ratio, the supported length used was 148 mm. In addition to the supported length, an overhanging length of 46 mm was added to the supported length from each side to ensure the bar would not slip off the supports during testing. The total length of the bars was 240 mm.

The testing apparatus consisted of two roller supports each having a radius of 10 mm, and a loading nose that has a cylindrical surface with a diameter of 10 mm connected to a Universal Testing Machine that has a controlled displacement rate. Figure 5 shows the flexure test setup just before the start of testing.

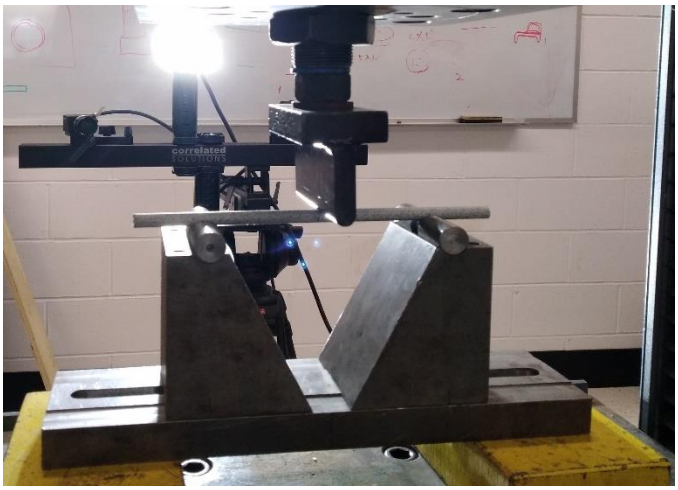

Figure 5- Flexure test setup

3.1.2 Loading Rate

The rate of Crosshead motion was calculated according to ASTM D790-17 [11] using the following equation:

$R = ZL^2/6d$,

Where, R = rate of crosshead motion (mm/min)

L = supported span = 148 mm

d = bar diameter = 9.25 mm

Z = strain rate of the outer fiber = 0.01 min^{-1}.

To meet the specified strain rate of 0.01 min^{-1} crosshead motion rate used was 3.95 mm/min.

3.1.3 Test Matrix

Table 1 below illustrates the flexure test matrix, showing the number and the dimensions of the bars tested, and the cross-head motion rate used.

Table 1- Flexure test matrix

Number of Specimens	Supported Length (mm)	Total Length (mm)	Cross-head motion rate (mm/min)
5	148	240	3.95

3.2 Compression Test

The most used standard test method to determine the compressive properties of GFRP bars is ASTM D695-10 "*Standard Test Method for Compressive Properties of Rigid Plastics*" [12]. However, the mentioned test standard was not designed specifically to determine the compressive properties of GFRP bars. Consequently, the test method used was a slightly modified version of the test method that was proposed by Khorramian et al. [6].

3.2.1 Tested Specimens Number and Dimensions

Five specimens each having a diameter of 9.25 mm and a length of 20 mm, approximately twice that of the diameter, were tested.

3.2.2 Test Setup

The new testing method required us to manufacture the testing apparatus. Two square plates each having dimensions of 75 mm x 75 mm x 8.5 mm were manufactured, and each plate had a hole on its bottom to allow the loading heads of the testing machine press

through them. The bar was held on a cylindrical base that had a diameter of 25.4 mm and a narrower diameter at its top equal to the diameter of the bar. The bar was held between the two cylindrical bases that were welded to the square steel plates. Threaded rods were used to help in making the specimen perfectly aligned by keeping the two plates leveled with each other. After setting up the testing apparatus the specimens were ready to be tested using a loading rate of 0.6 mm/min for a strain rate of 0.03 min^{-1}. Figure 6(a) and Figure 6(b) show the compression test setup schematic drawing, and the test setup just before the beginning of testing respectively.

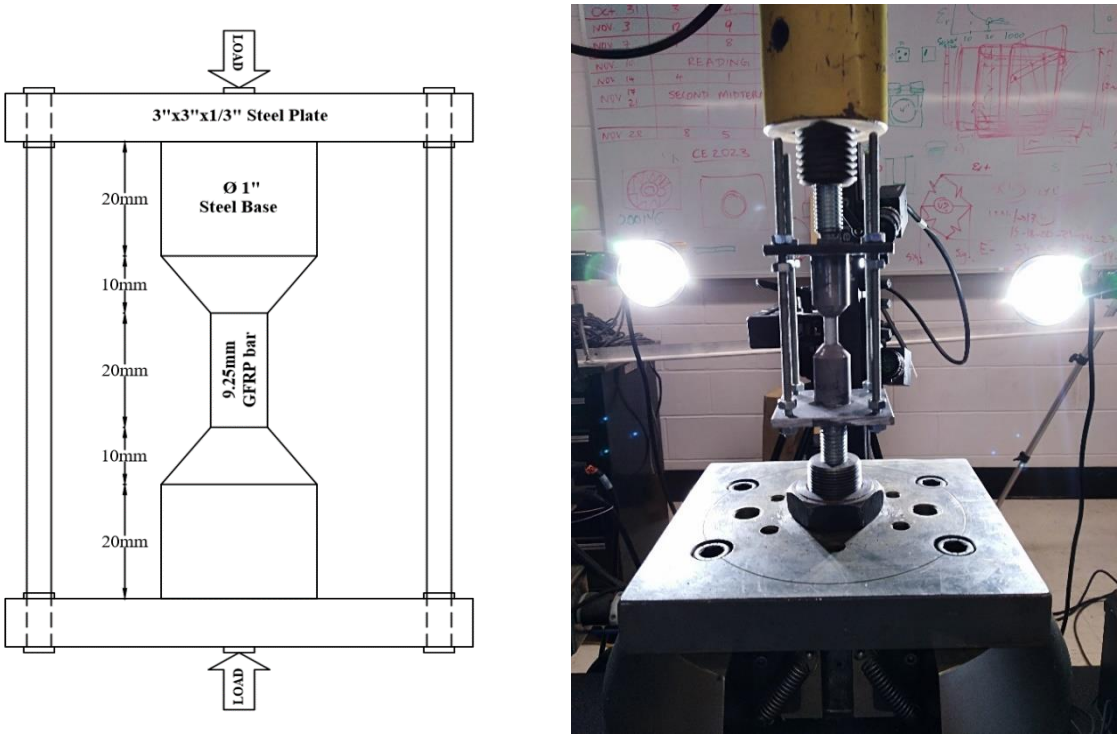

(a) **(b)**

Figure 6- (a) Compression test apparatus schematic (b) Compression test apparatus

3.2.3 Test Matrix

Table 2 below illustrates the flexure test matrix, showing the number and dimensions of the bars tested, and the loading rate used.

Table 2- Compression test matrix

Number of Specimens	Specimen Length (mm)	Specimen diameter (mm)	Loading rate (mm/min)
5	20	9.25	0.6

3.3 Tension Test

Inevitably, this test was the most challenging test among all three tests, due to the low shear strength that GFRP bars have compared to steel, which will cause immature failure if connected directly to the grips of a testing machine. ASTM developed a standard test method to determine the tensile properties of FRP bars, ASTM D7205/7205M - 06 *"Standard Test Method for Tensile Properties of Fiber Reinforced Polymer Matrix Composite Bars"* [13], which solved the problem of connecting the bars to the testing machine, and allow the test to progress until failure occurs allowing the bars reach their ultimate tensile strength.

3.3.1 Tested Specimens Number and Dimensions

ASTM D7205/7205M [13], specifies five specimens should be tested, unless fewer specimens yielded valid results. Due to the time the specimens take to be prepared and tested along with the uniformity of the results, only three specimens were tested in tension.

The overall length of the specimens consisted of the free length (gauge length) and two times the anchorage length, where, the former was 220 mm and the latter was 270 mm making the total length of the specimen becomes 760 mm. The free length used was less than the free length specified by the test standard, ASTM D7205/7205M – 06 [13] specifies the bar free length to be not less than 380 mm nor less than 40 times the effective bar diameter, the free length was reduced to what was required to make the tested specimen fit between the loading heads of the testing machine.

3.3.2 Test Setup

Steel anchors, consisting of a length of steel pipe, were used to connect a GFRP bar to the testing machine. ASTM D7205/7205M [13] summarizes the minimum dimensions of the steel anchors according to the specimen's diameter. Table 3 below shows a table summarizing the dimensions of the steel anchors according to the dimeter of the bar taken from ASTM D7205/7205M – 06 [13]. Anchors with inner diameter of 20 mm and length of 300 mm were used, and holes were drilled in to them so they can be connected to the testing machine. The anchorage lengths of the bars were coated with epoxy before coating them with coarse sand that was passed through a 1.25 mm sieve and was retained by a 1.18 mm sieve. This was done to increase the friction between the bar and the expansive mortar that was used to connect the bars to the anchors.

Two types of expansive mortar were explored for use in connecting the bars to the anchors. The first of these, Betonamit, was selected because of its high availability in the market and high curing pressure of up to 83 MPa. This mortar was found to provide insufficient confinement pressure to restrain the bars from slipping in the anchors.

Betonamit was replaced by another mortar, Rockfrac, which has a higher curing pressure of 138 MPa. It was mixed with a water to mortar ratio of 0.30 as per the manufacturer's specifications, and then was poured inside the steel anchors in alternating days as Rockfrac requires a minimum time of 24 hours to set. A minimum total cure time of 7 days was provided prior to testing the specimens. The specimens were tested with a displacement rate of 1 mm/min as per the test standard.

Table 3- Recommended dimensions of test specimens and steel tubes [13]

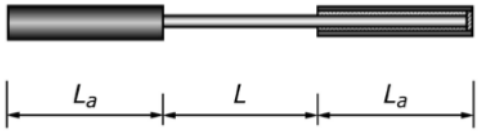

FRP bar type	Diameter of the FRP bar, d	Outside diameter of the steel tube	Minimal length of the steel tube, L_a
GFRP	6.4 mm [0.25 in.]	35 mm [1.38 in.]	300 mm [12 in.]
GFRP	9.5 mm [0.38 in.]	35 mm [1.38 in.]	300 mm [12 in.]
GFRP	13 mm [0.50 in.]	42 mm [1.63 in.]	380 mm [15 in.]
GFRP	16 mm [0.63 in.]	42 mm [1.63 in.]	380 mm [15 in.]
GFRP	19 mm [0.75 in.]	48 mm [1.88 in.]	460 mm [18 in.]
GFRP	22 mm [0.88 in.]	48 mm [1.88 in.]	460 mm [18 in.]
GFRP	25 mm [1.00 in.]	48 mm [1.88 in.]	460 mm [18 in.]
GFRP	29 mm [1.13 in.]	48 mm [1.88 in.]	460 mm [18 in.]
GFRP	32 mm [1.25 in.]	75 mm [2.95 in.]	800 mm [32 in.]
CFRP	9.5 mm [0.38 in.]	35 mm [1.38 in.]	460 mm [18 in.]

Figure 7(a) and Figure 7(b) below show the GFRP bars after having their anchorage lengths sand coated, and an embedded GFRP bar inside of a steel anchor after the setting of the expansive mortar respectively.

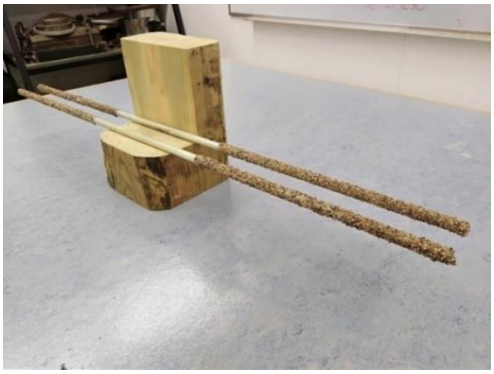

(a)

(b)

Figure 7- (a) Sand coated GFRP bars (b) Steel anchor filled with expansive mortar

Figure 8 and Figure 9 below show a prepared GFRP bar ready for testing, and a GFRP bar connected to a universal testing machine just before the start of testing.

Figure 8- GFRP bar embedded in steel pipes curing

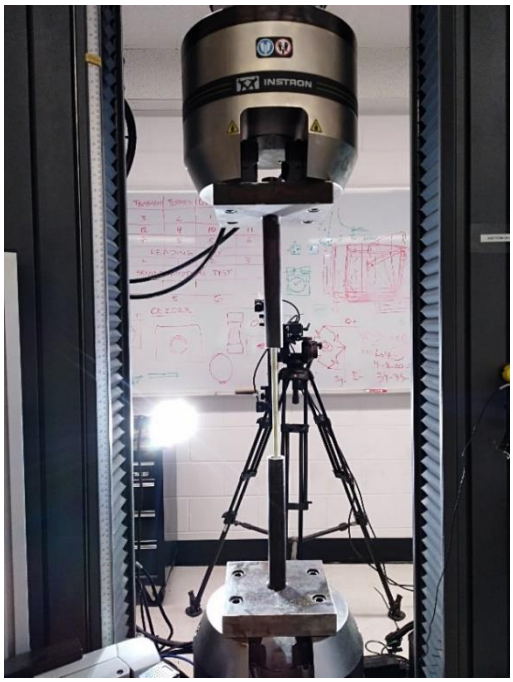

Figure 9- GFRP bar installed in to the testing machine

3.3.3 Test Matrix

Table 4 below illustrates the tension test matrix, showing the number of bars tested, dimensions of the bars and anchors, and the loading rate used.

Table 4- Tension test matrix

Number of Specimens	Free Length (mm)	Anchorage Length (mm)	Total Length (mm)	Specimen Diameter (mm)	Outer Diameter (mm)	Inner Diameter (mm)	Loading rate (mm/min)
3	220	270	760	9.25	30	20	1.0

4. Compression Analysis

4.1 Failure Mechanism

The failing mechanism observed in all tested specimens were very similar. Where, the type of failure was a brittle failure occurred due to the crushing of fibres and not their buckling. The materials behaved as linear-elastic, showing no yielding or any ductile behavior prior to failure. Figure 10 and Figure 11 show the failed specimens, and the extracted longitudinal strain plots from DIC from the start of testing until failure respectively.

Figure 10- Failing mechanism in compression

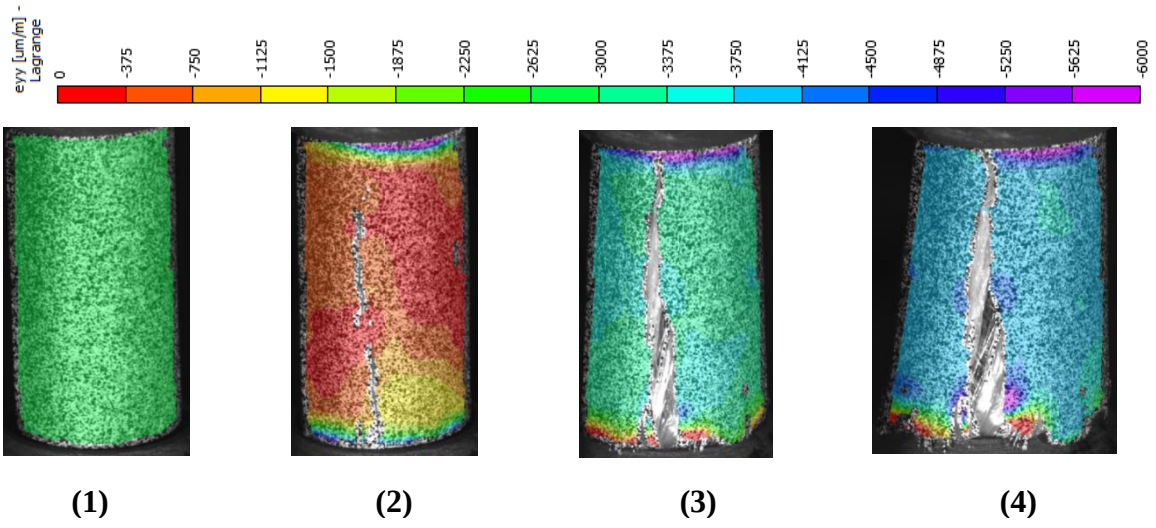

Figure 11- Longitudinal strain plots of a specimen from the start of testing until failure

Figure 12 and Figure 13 below show the brittle type of failure of GFRP bars in compression. The relationship between the load and displacement is linear until a sudden drop of load occurs indicating the occurrence of failure and showing no ductility capacity. Where, the displacement is the relative displacement between the end points of the extensometer. Similarly, Figure 13 shows a linear increase in strain as time increases until an abrupt drop in strain occurs indicating failure.

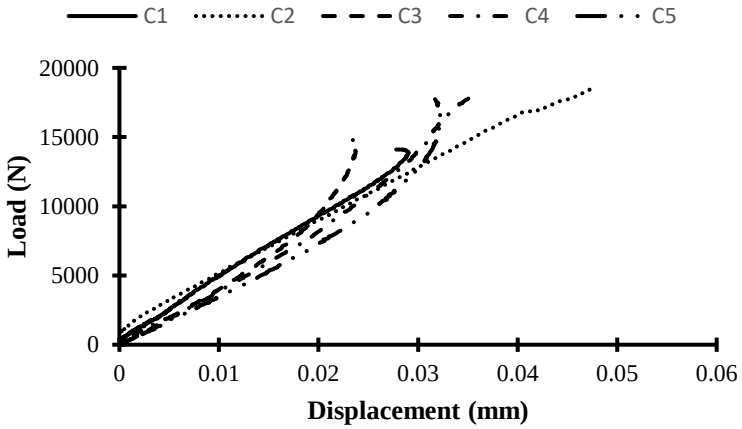

Figure 12- Compressive load-displacement relationship

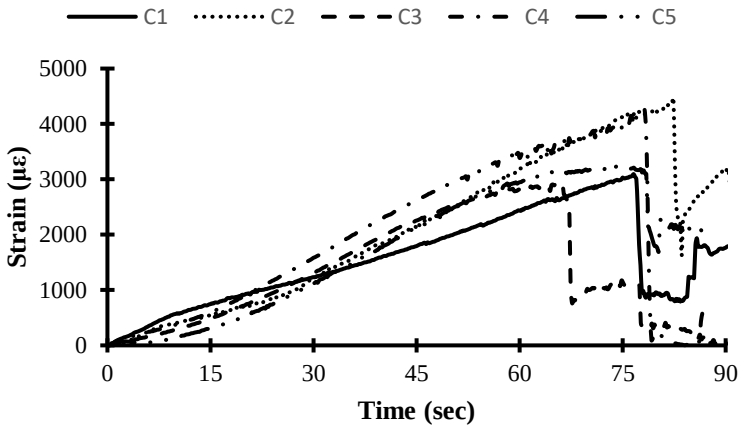

Figure 13- Compressive strain variation with respect to time

4.2 Load Eccentricity and Strain Variations

4.2.1 Compressive Load Eccentricity

The strain field data from the DIC measurements was used to determine if the axial load was concentric or eccentric. This knowledge would then be used to determine the average strain location in the compression member. Using the DIC software, three inspection lines were drawn on each tested specimen. Two lines (L_1 and L_2) were drawn on each side of the specimen, while the third line (L_0) was drawn between them. The strain data along each inspection line was extracted at three different loading stages (A-C) as shown in Figure 14.

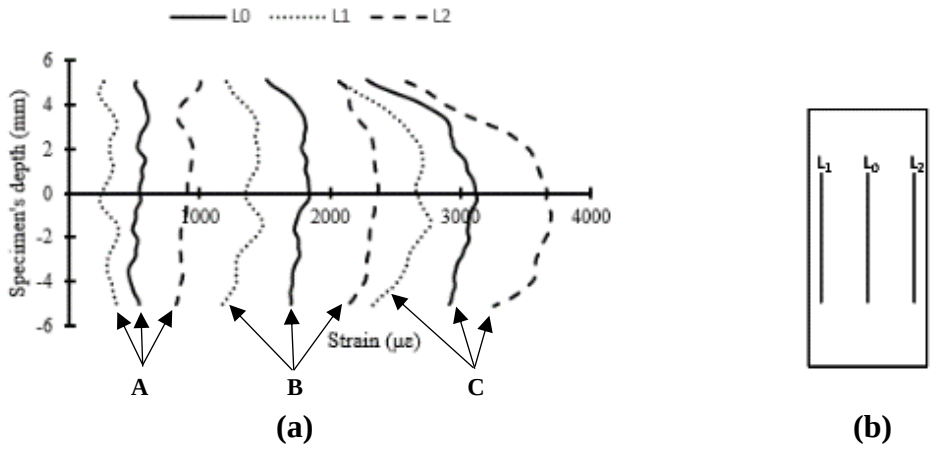

Figure 14- (a) Compressive strains along the inspection lines at different loading stages (b) Inspection lines locations

The strains along the three inspection lines were not aligned with each other implying that the load was not concentric. This means that the virtual extensometer used to average strains over the length should not be placed in the center of the specimen otherwise inadequate results will be obtained. Therefore, lines L_1 and L_2 were placed at each end of the bar and line L_0 was placed in a location that yields strain values that are approximately averaging the strains of lines L_1 and L_2 as shown in the plot of Figure 14.

The location that averaged the strains of lines L_1 and L_2 is the location where the extensometer was placed, and all further analysis and calculations performed were using the data extracted at that location.

4.2.2 Strain Variations

Figure 15 shows strain plots at four different loading stages extracted from DIC, and the variation of average strains with respect to the applied load plot that shows the corresponding loading stages of the strain plots. It can be observed by looking at the strain plots that high strains are generated near the ends of the bar, which was expected due to the high pressure generated at the point of contact between the testing machine loading heads and the bar. Apart from the bar's ends, strains were found to be larger in the right hand side compared to that in the left hand side, implying that the applied load is located on the right hand side rather than being located in the center proving load eccentricity that the performed test delivered.

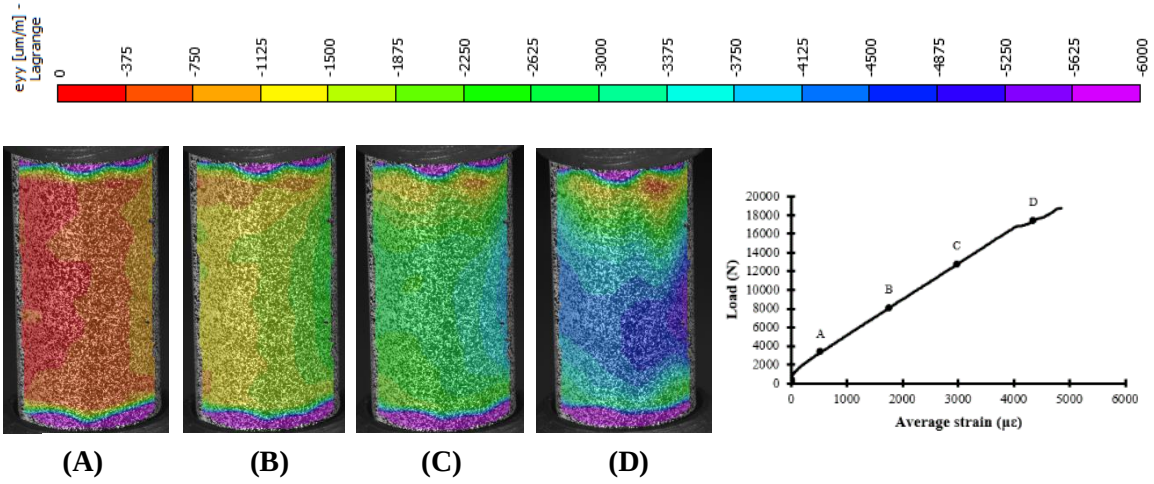

Figure 15- Compressive strain variations at different loading stages

4.3 Compressive Modulus of Elasticity

To determine the modulus of elasticity of GFRP bars in compression, the stress needs to be computed. Since, the performed compression test is a pure axial test (the small moment generated due to eccentricity is neglected and strains are measured at the average location), the stress is calculated as the applied force divided by the cross-sectional area of the bar, giving:

$\sigma_c = \frac{4P}{\pi d^2}$, where, σ_c = Compressive Stress, MPa.

P = Applied Force, N.

d = diameter of the bar, mm.

The compressive modulus of elasticity is defined as the slope of the compressive stress-strain curve. Since, the strain data was extracted at the location that gave average strain, the data couldn't yield a perfectly linear stress-strain curve. Figure 16 below shows the procedure to compute the stress-strain curve slope. So, to compute the compressive modulus of elasticity, the linear part of the stress-strain curve (CD in Figure 16) needs to be extended so that it intersects with the strain axis. That intersection is the corrected zero strain (Point B in Figure 16) by which all strains must be measured from.

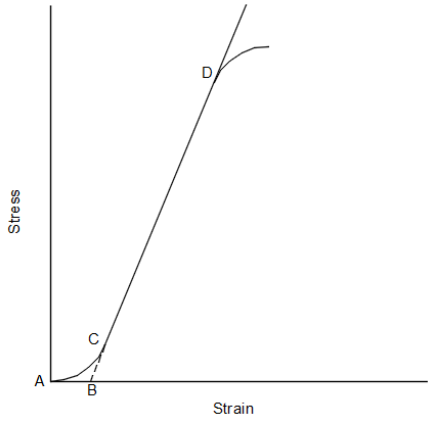

Figure 16- Stress-strain slope determination

Modulus of elasticity is then calculated by dividing the stress at any point along line (CD) or its extension by its corresponding strain measured from the corrected zero strain ($E= \frac{\sigma_i}{\varepsilon_i - \varepsilon_B}$).

4.4. Compression Test Results

Figure 17 shows the stress-strain curves that wasn't perfectly linear, and Figure 18 shows the idealized stress-strain relationship, which represents the linear part of the curves in Figure 17. The origin of the idealized stress-strain curves in Figure 18 are the corrected zero strain of the curves in Figure 17. Therefore, the compressive modulus of elasticity for each specimen was computed using the idealized stress-strain relationship, by dividing any stress by its corresponding strain.

4.4.1 Stress-Strain Curves

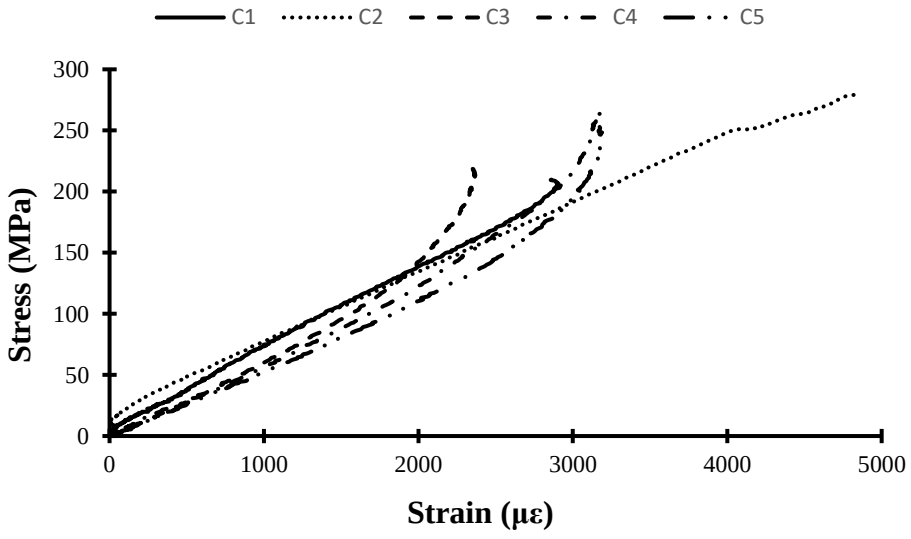

Figure 17- Compressive stress-strain curves

4.4.2 Idealized Stress-Strain Relationship

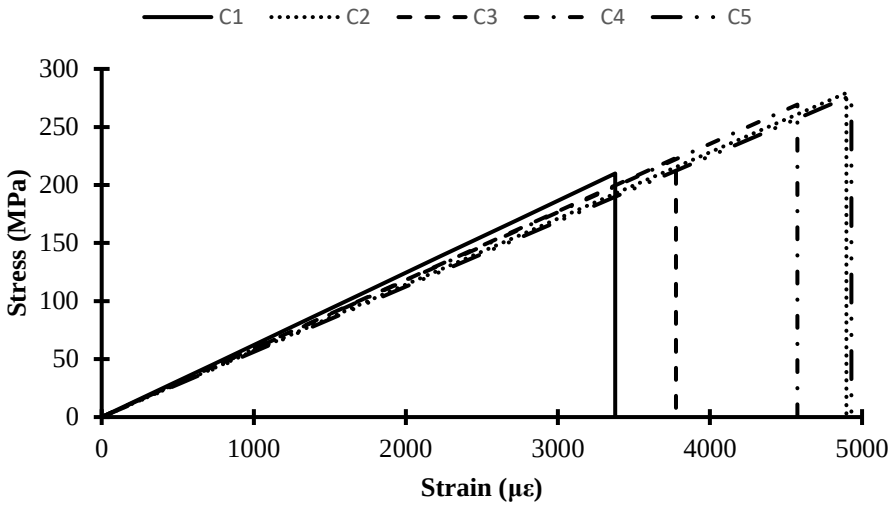

Figure 18- Idealized stress-strain relationship in compression

4.4.3 Compression Test Results Summary

Table 5 summarizes the results obtained from the compression test, showing the ultimate load, ultimate stress, and the compressive modulus of elasticity for each specimen, in addition to, the average and the standard deviation of all specimens.

Table 5- Compression test results summary

Specimen	P_{max} (KN)	σ_{max} (MPa)	E (GPa)
C1	14.106	209.907	62.163
C2	18.769	279.304	57.034
C3	15.007	223.321	59.135
C4	18.094	269.256	58.857
C5	18.626	277.163	56.222
Average	16.920	251.790	58.682
Standard deviation	2.196	32.675	2.298

5. Tension Analysis

5.1 Failure Mechanism

The failing mechanism observed from the performed tension test was characterized in the splitting of the fibres in the free length of the bars. Furthermore, the type of failure was a brittle type of failure as expected, where, the splitting of the free length fibres occurred abruptly without showing any yielding. Figure 19 shows the failing mechanism of the bars in tension, and Figure 20 shows a series of images extracted from DIC for a specimen during the tension test, which shows that failure started in the free length.

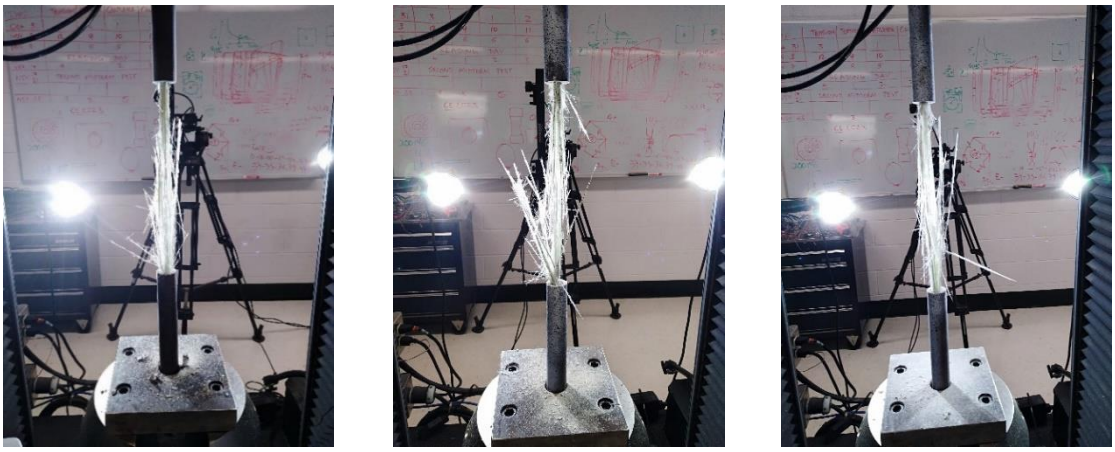

T1 **T2** **T3**

Figure 19- Failing mechanism in tension

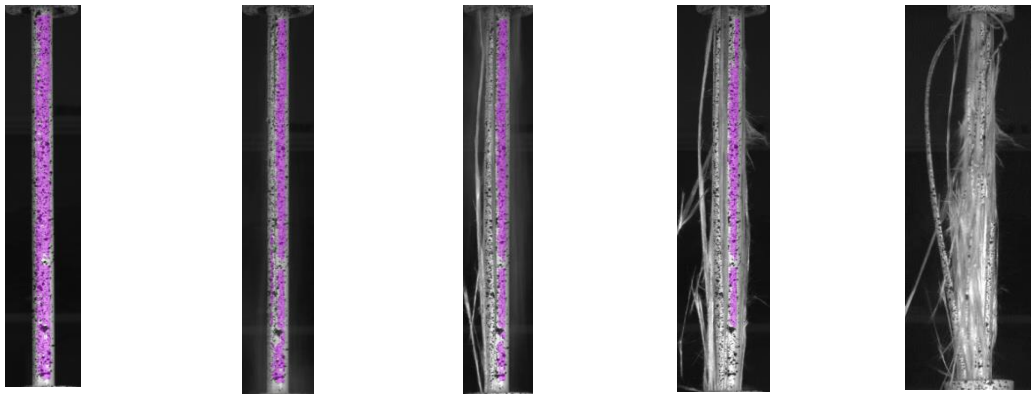

Figure 20- Failing mechanism captured by DIC

The brittle failure of the GFRP specimens in tension is shown in Figure 21, which illustrates the load-displacement relationship for the tested specimens, where, the relation between the load and displacement was linear until an abrupt drop in the load occurred indicating the occurrence of failure without showing any plateau or any kind of ductile behavior. The horizontal lines drawn on the plot represents the maximum load that was carried by specimens T2 and T3. In specimens T2 and T3, the DIC strain and displacement measurements were not able to be completed all the way to maximum load due to the progressive fibre failures that obscured the images preventing optical measurements.

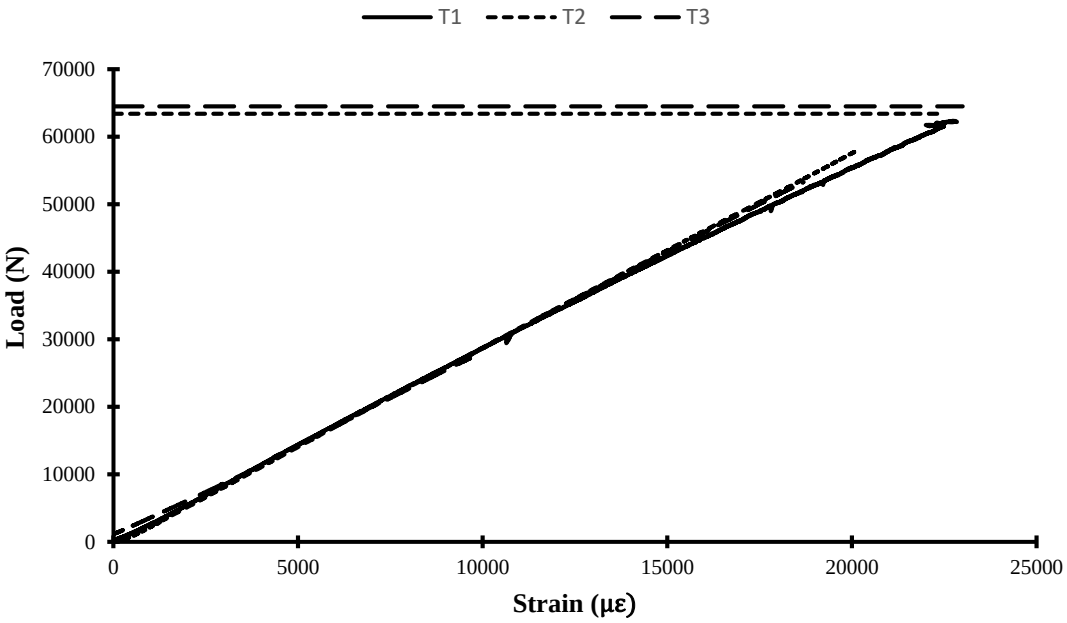

Figure 21- Tensile load-strain relationship

5.2 Load Eccentricity and Strain Variations

5.2.1 Tensile Load Concentricity

Similar to the compression test, it is important to determine the type of loading that the performed tension test method delivered to know whether the load is concentric or eccentric in order to determine the location where the strain data should be extracted from. Inspection lines were drawn on the specimen and strain data was extracted at the location of the inspection lines to check if the strain data along the length of the specimen at the different locations are aligned with each other indicating load concentricity, or they indicate load eccentricity.

Figure 22(a) and Figure 22(b) show the tensile strains along the length of the specimen on the three different locations at four different loading stages, and the locations of the inspection lines respectively. It can be clearly observed that the strains at the different locations are concurrent indicating load concentricity. Therefore, the extensometer was placed at the center of the specimen to extract all the data required to proceed with the analysis.

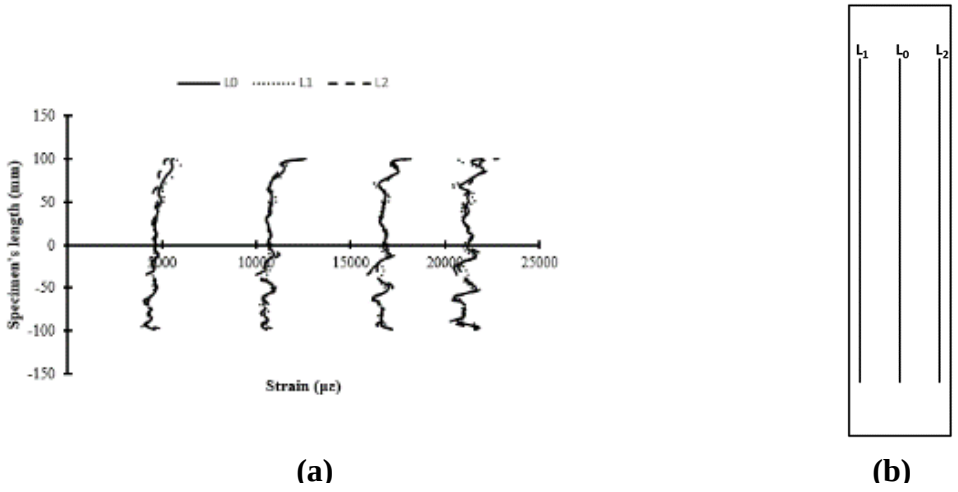

Figure 22- (a) Tensile strains along the inspection lines (b) Inspection lines locations

5.2.2 Strain Variations

Figure 23 shows the longitudinal strain field plots at four different loading stages extracted from DIC, in addition to the load-strain graph that shows the corresponding loading stages of the strain plots, where, the longitudinal strain is the strain extracted using an extensometer which had a length equals to the length of the strain field shown in the plots. The uniformity of the strain fields over the length is apparent in Figure 23 A-D as shown by the uniform colour. Figure 23 D shows the incipient failure zone near the centre of the bar as a high strain location visible in the colour map. The strains recorded in the loading stages for Figure 23, A through D, were approximately 4,500με, 10,000με, 18,000με, and 23,000με, which was the ultimate strain the specimen reached.

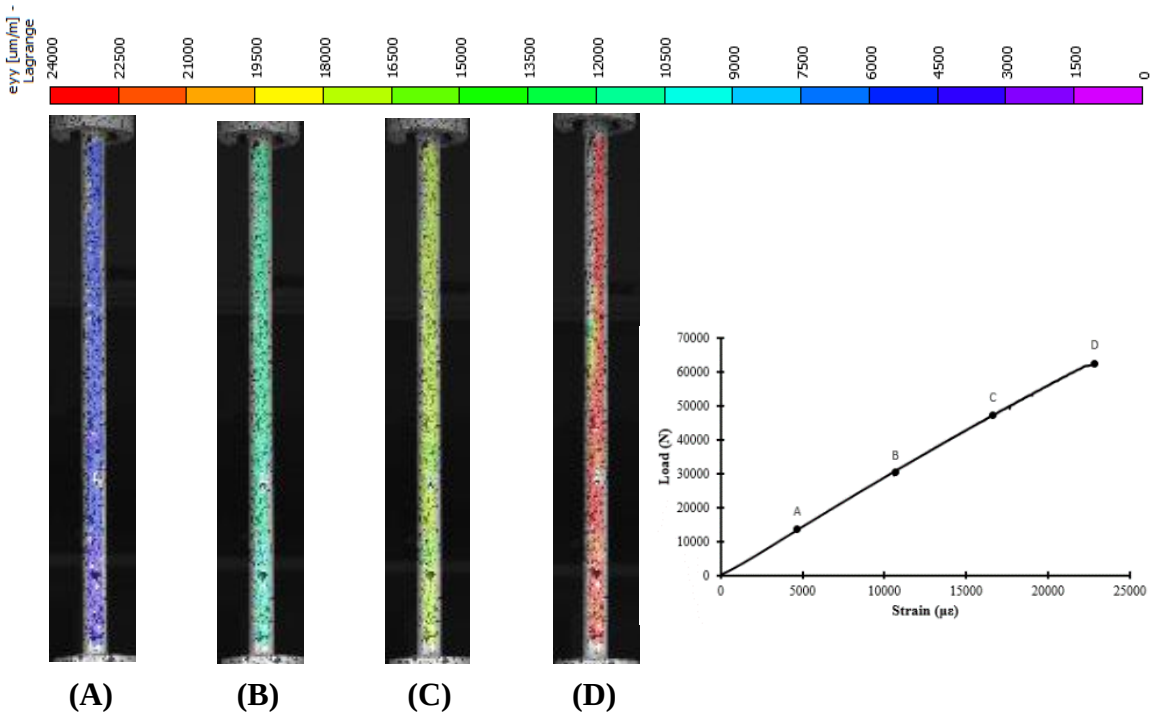

Figure 23- Tensile strain variations at different loading stages

Figure 24 shows the strain distribution along the specimen's length at the four different loading stages that were presented in Figure 23. Strain uniformity can be observed by looking at stages (A), (B), and (C), where, approximately equal strain values were found at each point along the length of the specimen. On the other hand, the strains in loading stage (D), just prior to failure, had significant variation over the length indicating the presence of stress concentrations leading to failure.

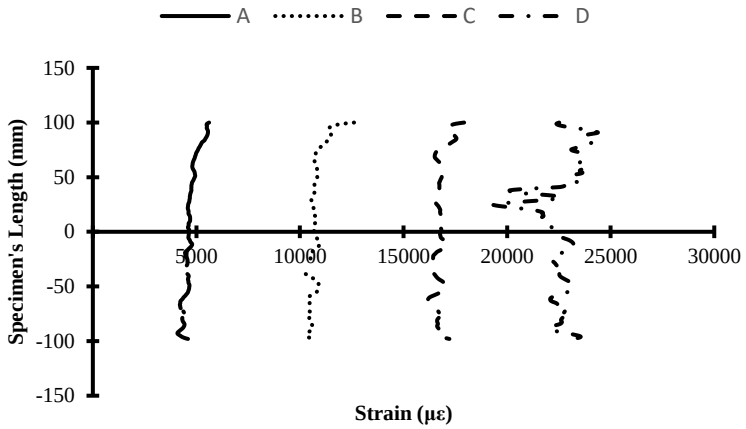

Figure 24- Tensile strain with respect to specimen's length

5.3 Tensile Modulus of Elasticity

Similar to compression, the tensile modulus of elasticity is the slope of the tensile stress-strain curve. Unlike compression, since the stress-strain curve in tension was completely linear there is no need to determine a corrected zero strain. Since the performed tension test was a pure axial test, stress is computed as the applied force divided by the cross-sectional area of the bar, as follows:

$\sigma_t = \frac{4P}{\pi d^2}$, where, σ_t = Compressive Stress, MPa.

P = Applied Force, N.

Figure 25 shows the stress-strain curves for all three tested specimens in tension, where, a linear stress-strain relationship is observed.

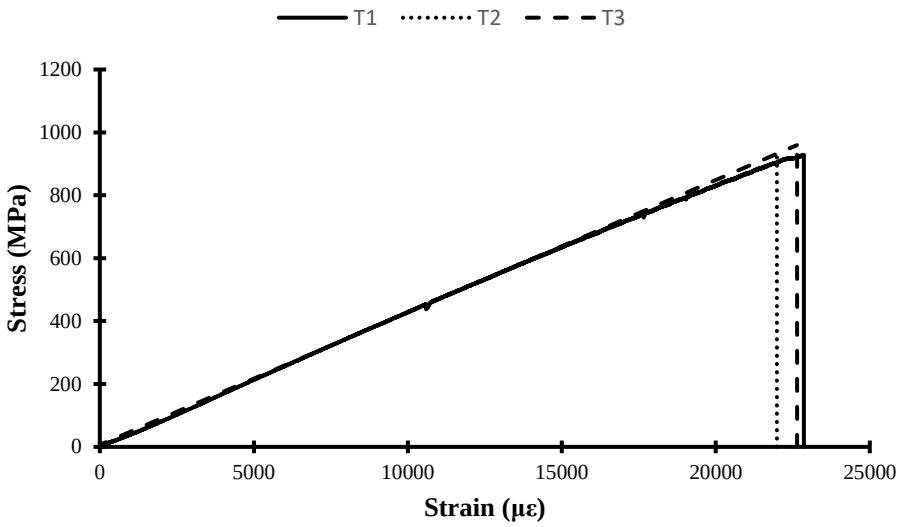

Figure 25- Tensile stress-strain relationship

5.4 Tension Test Results

Table 6 summarizes the results obtained from the tension test, showing the ultimate load, ultimate stress, and the tensile modulus of elasticity for each specimen, in addition to, the average and the standard deviation of all specimens.

Table 6- Tension test results summary

Specimen	P_{max} (KN)	σ_{max} (MPa)	E (GPa)
T1	62.363	928.018	41.408
T2	63.384	943.202	43.192
T3	64.477	959.472	42.111
Average	63.408	943.564	42.237
Standard Deviation	1.057	15.730	0.899

6. Flexure Analysis

As mentioned in **section 3.1**, five GFRP bars were tested in a 3-point bending test to determine the behavior of GFRP bars in flexure. The experimental results of those bars are presented here.

6.1 Failure Mechanism

The failing mechanism observed was the same in all the five tested specimens, where, all tested specimens failed in compression (crushing in the top fibres of the bar) while the bottom (tension) fibres remained undamaged. Figure 26 shows the longitudinal strain field distribution plots at four different loading stages. The strain distribution at the load point (maximum moment) moves from compression in the top fibres through zero near the mid-height and to tension at the bottom. This is what is expected for flexural strain distributions. Which shows the gradual disappearance of color in the top fibres, indicating damage forming and a loss of ability to optically measure strain. This location coincides with the compression failure location. (In the appendix, the variation of compressive and tensile strain with respect to time due to bending can be found in Figure 41 - Figure 45).

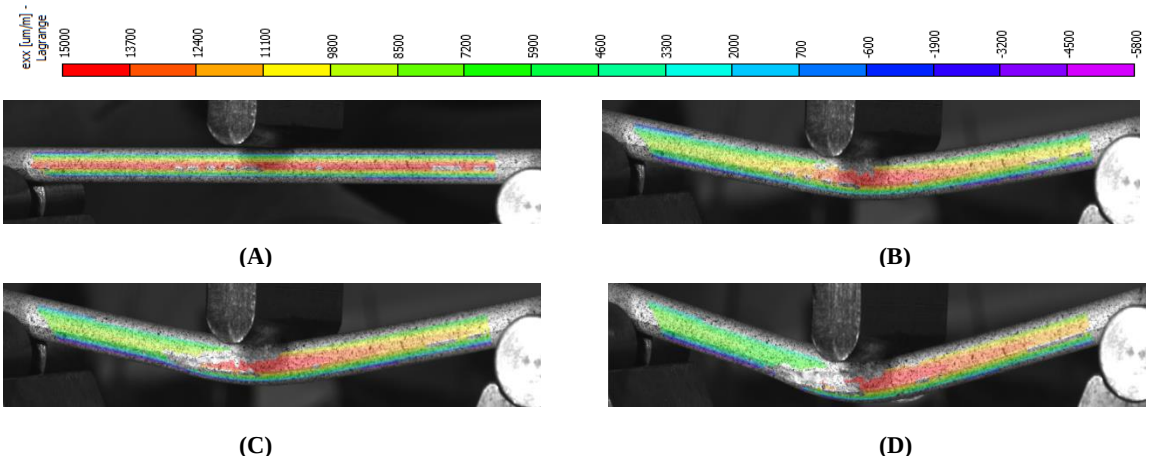

Figure 26- Flexural longitudinal strain captured by DIC

Figure 27 shows the failing mechanism of the tested bars in flexure, showing the crushing of fibres on only one side of the bars which was the compression side.

Figure 27- Failing mechanism in flexure

The type of failure occurred from the flexural test was a brittle type of failure. That can be observed by looking to Figure 28, the load-displacement relationship of the tested GFRP bars in flexure. In this figure it is apparent that the response is linear up to the maximum load where failure occurs.

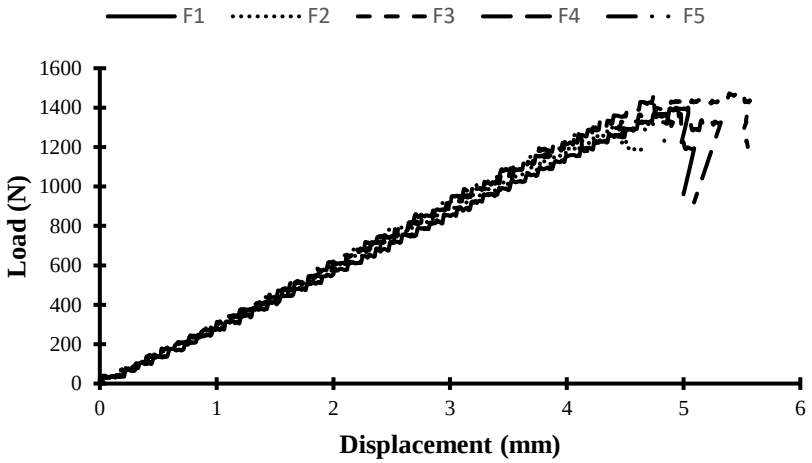

Figure 28- Flexural load-displacement relationship

6.2 Flexural Neutral Axis

The analysis results for both the tensile and the compressive tests yielded different modulus of elasticity for each loading scenario, where, the modulus of elasticity in compression was larger than that in tension by 1.41 times. The difference between the elastic moduli indicates that the location of the flexural neutral axis cannot be at the center of the bar's cross-section. Moreover, since the modulus of elasticity in compression is larger than that in tension, the neutral axis is expected to be shifted towards the fibres undergoing compression (top fibres). To investigate the location of the neutral axis, flexural strain data was extracted at different loading stages along the depth of the specimen as shown in Figure 29. The strain along the depth of the section was largely linear. This confirms that plane strain over the section's depth is a valid assumption to use in sectional analysis.

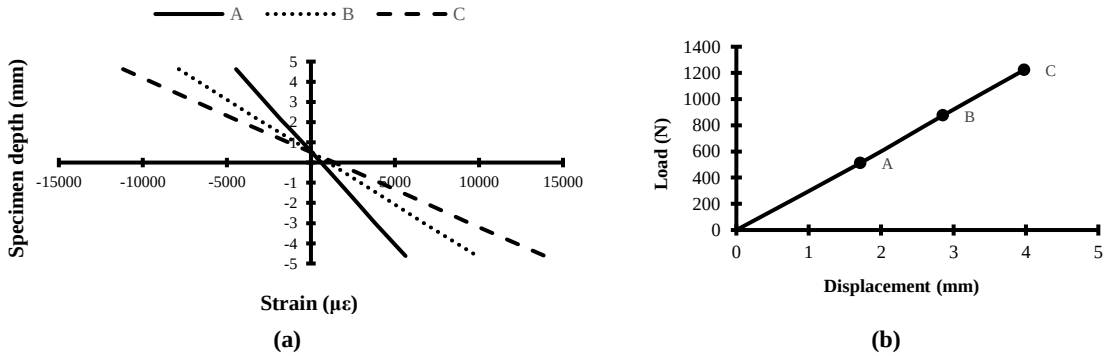

Figure 29- (a) Strain diagrams at different loading stages (b) Load-displacement

Figure 29 shows that the neutral axis is not located at the center of the specimen at all loading stages, moreover, the figure clearly shows that the neutral axis was shifted upward towards the compression face (top fibres) of the bar as expected. The actual location of the neutral axis, in addition to the compressive and the tensile elastic moduli can be used to check horizontal equilibrium, and check how the computed moment can be compared to the applied moment.

6.3 Moment-Curvature Relationship

The moment-curvature (M-Φ) relationship of a section is a measurement of its rigidity and ductility capacity. Measuring this relationship confirms if the type of a material is brittle or ductile, and directly provides the combined sectional and material properties of modulus of elasticity and moment of inertia (EI) as the slope of the elastic region of the M-Φ curve. By considering the longitudinal strain along the depth of the tested GFRP bar to be linear, curvature (Φ) can be calculated as the ratio between the strain at the extreme fibres and the neutral axis depth. Furthermore, since the performed flexural test was a 3-point bending test, the maximum applied moment can be determined as the applied force at the center of the bar multiplied by ¼ of the bar's supported length. Figure 30 shows a schematic figure for the linear strain over the section's depth, showing the curvature and strains at extreme fibres.

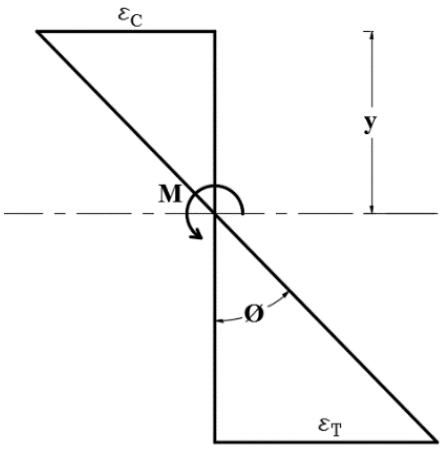

Figure 30- Strain linear distribution diagram along specimen's depth

$\Phi = \frac{\varepsilon}{y}$ Where, ε= Strain at the extreme fibres.

y= Neutral axis depth.

$M = \frac{PL}{4}$ Where, M= moment applied (KN.mm)

P= Applied Load (KN)

L= Supported span length (mm)

Figure 31 illustrates the variation of curvature with respect to the applied moment for all five tested specimens. As it can be observed in Figure 31, the relationship between the curvature and applied moment is linear from the beginning of loading up until failure occurs. Furthermore, there is no flexural ductility observed as evident by the brittle failure at maximum moment.

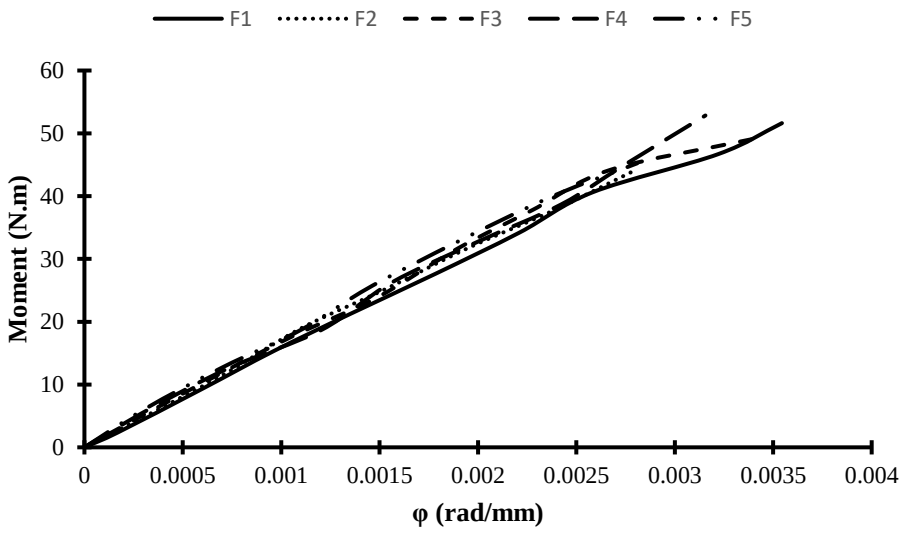

Figure 31- Moment-curvature relationship

The rigidity (EI) of a member is defined as the slope of moment-curvature as expressed in the following relationship:

$EI = \frac{M}{\Phi}$

Table 7 summarizes the flexural rigidity (EI) of all tested specimens in flexure, in addition to, the average and standard deviation.

Table 7- Flexural stiffness summary

Specimen	EI (N.m^2)
F1	15.649
F2	16.284
F3	16.678
F4	16.690
F5	17.601
Average	16.581
Standard Deviation	0.710

6.4 Sectional Analysis

A layer-by-layer sectional analysis was performed by enforcing force equilibrium along the cross-section of the bars while assuming planar sections to determine the moment resistance of the specimens and compare them with the applied moments. To perform the sectional analysis, the circular cross-section was divided in to small rectangular slices that have a width of b_i and thickness t_s. Since the cross-section of the bars had a circular shape, the width of each slice was variable from one location to another along the depth of the section. The width of each slice was defined using the equation of a circle, $x^2 + y^2 = r^2$. Where, **y** is the vertical distance to the center of the slice measured from the center of the cross-section of the bar, **r** is the radius of the bar, and **x** is half the width of the slice. Therefore, the width of each slice was found to be $b = 2.\sqrt{r^2 - y^2}$.

Figure 32 shows the cross-section of a GFRP bar and the stress distribution along the depth of the section showing all parameters that represent stresses and dimensions.

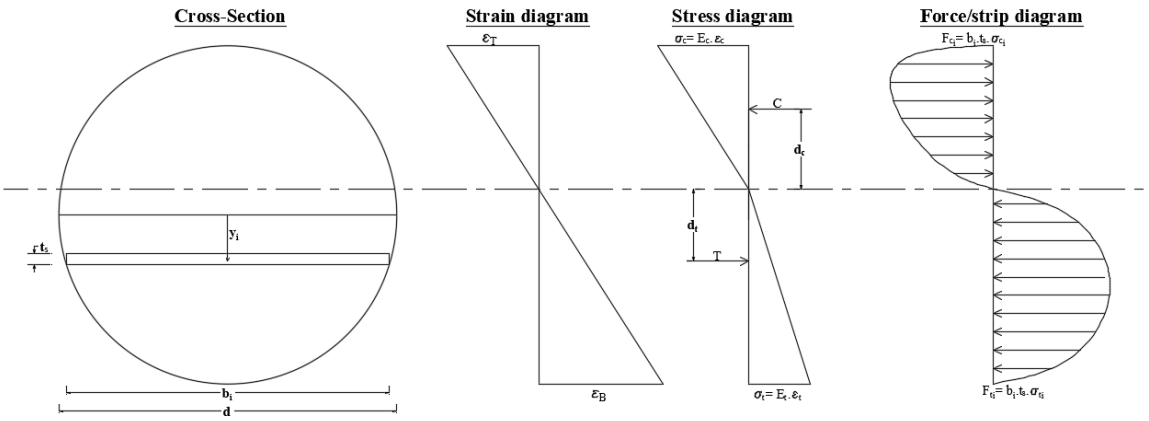

Figure 32- Layer by layer sectional analysis

From the obtained tensile and compressive results, the compressive and tensile stresses in each slice was calculated by using the flexural strains and the elastic moduli from the tests mentioned earlier. Where, the stresses are computed as follows:

$\sigma_c = E_c.\varepsilon_c$, Where, E_c = Compressive modulus of elasticity

ε_c = Compressive strain

$\sigma_t = E_t.\varepsilon_t$, Where, E_t = Tensile modulus of elasticity

ε_t = Tensile strain

From the computed stresses in the slices, the force generated in each slice can be calculated by multiplying the stress in the slice by its area. Where, the total compressive and tensile forces are computed as follows:

$C = \int \sigma_c .b(y)dy$

$T = \int \sigma_t .b(y)dy$

After calculating the total compressive and tensile forces in the cross-section, the moment arms of these forces were computed. The moment arms, with respect to the location of the neutral axis of the specimen, were found by using the following equations:

$d_c = \frac{\Sigma C_i y_i}{C}$ and $dt = \frac{\Sigma T_i y_i}{T}$; where

C = Total Compression force

T = Total Tension force.

d_c = distance between the total compressive force and the specimen's center.

d_t = distance between the total tensile force and the specimen's center.

C_i = Slice's Compression force.

T_i = Slice's Tension force.

y_i = slice's moment arm measured from the center of the specimen.

The total moment arm between the tension and compression force in the cross section was found as:

$d = d_c + d_t$

And the moment resistance was computed then as follows:

$M_r = T.d$

6.5 Sectional Analysis Example

An example layer-by-layer sectional analysis was performed on a specimen at different loading stages to check equilibrium on each stage. It is important to note that small numerical errors are expected in the analysis because experimental data is used in the process. In this example, the circular cross section of the specimen was divided in to 4000 rectangular slices each having a thickness $\mathbf{t_s}$ of d/4000 and width $\mathbf{b_i}$.

6.5.1 Experimental Flexural Strain Data

A plane strain assumption was made that resulted in the strain along the depth of the specimen being linear. The strain at the center of each slice were computed by interpolating from the compressive and tensile strains at the extreme fibres. Additionally, location of the neutral axis and the distance to the center of the slices measured from the center of the specimen were found through interpolation.

Table 8 and Figure 33 below show the experimental data at the different loading stages in this analysis.

Table 8- Loading stages experimental data

Stage	ε_T (με)	ε_c (με)	y_0 (mm)	$M_{applied}$ (KN.mm)
A	5652.224	-5092.345	0.241	18.724
B	9722.150	-8701.575	0.256	32.649
C	13512.452	-11886.378	0.296	44.878

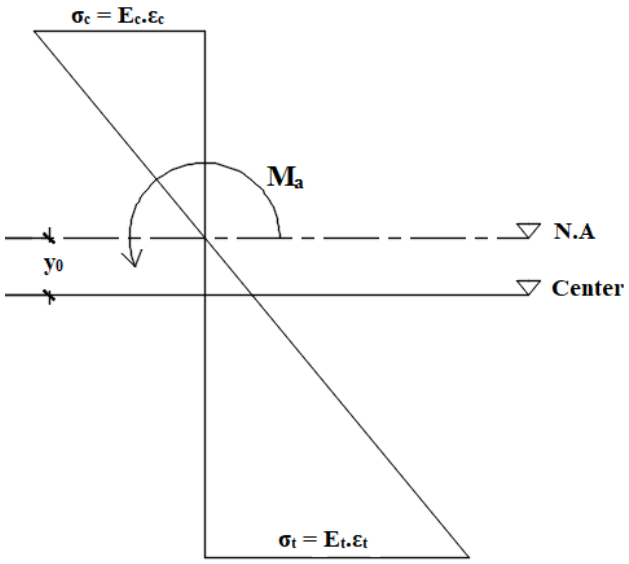

Figure 33- Sectional analysis example data

6.5.2 Horizontal Equilibrium Check

Horizontal equilibrium is achieved when the total tension force and total compression force equal each other. However, due to experimental data errors and to assumptions made in the calculations such as considering the strain distribution along the depth of the specimen to be completely linear, small numerical errors may occur. The stress in each slice, whether it is under tension or compression, was computed as the average tensile or compressive modulus of elasticity multiplied by the flexural strain at the central location of the slice. Figure 34 shows the stress distribution across the depth of the section at the three different loading stages.

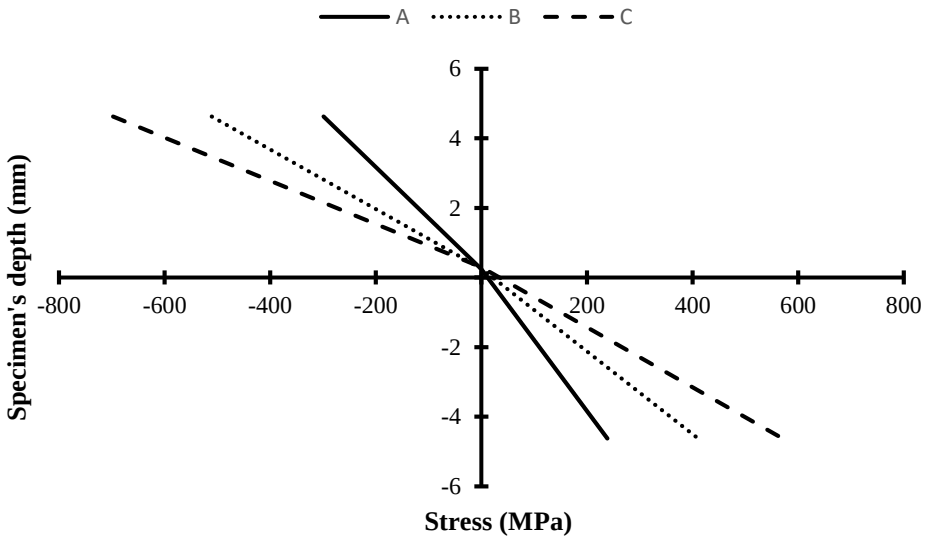

Figure 34- Stress distribution along the specimen's depth

The stress distribution obtained along the specimen's depth had a bi-linear shape as shown in Figure 34, which was due to the difference between the tensile and compressive moduli of elasticity. The tensile and compressive forces in the slices were computed by multiplying the stress in the slice by its area. After having calculated the force in each slice, the total

tensile and total compressive forces were computed by summing the forces in the slices under compression and those under tension separately. Table 9 below shows the total tension forces, total compression forces, and the difference between them at each loading stage.

Table 9- Horizontal equilibrium check

Stage	T	C	% difference
A	3.646	3.962	8%
B	6.298	6.738	7%
C	8.850	9.090	3%

As shown in Table 9, there was a small difference between the forces, where, the difference did not exceed 10% at the early loading stage, and was decreasing as the specimen was loaded more until it reaches only 3% at loading stage (C) (just before failure occurred). Figure 35 below shows the force/strip variation along the depth of the section.

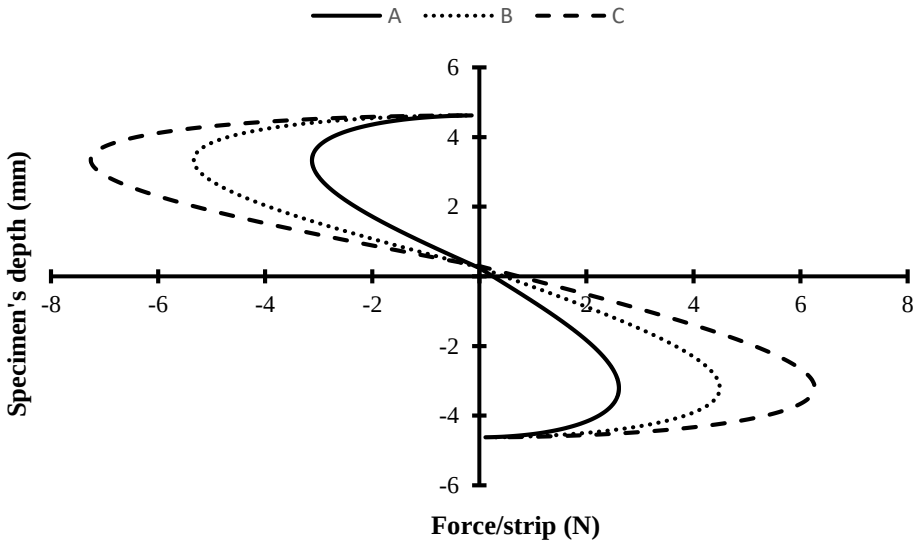

Figure 35- Force/strip for a strip thickness of d/4000

6.5.3 Total Forces Locations

As mentioned before, the location of the tension and compression total forces were computed as the ratio of the sum of moments in the slices, measured with respect to center of the specimen, and the total forces. So, the moment arm distance (the distance between the total forces) was then computed as the sum of the distance to the total compression force and total tension force locations measured from the center of the specimen. Making the moment arm distance $d = d_c + d_t$. Table 10 summarizes the distance from the center of the specimen to the location of the tensile and compressive forces, along with the moment arm used to compute the moment resistance at each loading stage.

Table 10- Locations of total forces measured from the center of the specimen

Stage	$\Sigma T_i.y_i$ (KN.mm)	$\Sigma C_i.y_i$ (KN.mm)	d_t (mm)	d_c (mm)	d (mm)
A	9.594	11.166	2.631	2.818	5.449
B	16.535	19.030	2.625	2.824	5.450
C	23.099	25.812	2.610	2.840	5.450

6.5.4 Moment Resistance Calculation

Moment resistance, Mr, is the maximum moment the section can be able to resist and it is defined as the total compression or tension force multiplied by the moment arm. Since the total tensile and compressive forces were not exactly equal and had a small difference between them, the total tensile force was used in computing M_r. Table 11 shows both the applied moment and the computed moment resistance along with the difference between the two moments at each loading stage.

Table 11- Moment resistance check

Stage	M_r	$M_{applied}$	% difference
A	19.870	18.724	6%
B	34.323	32.649	5%
C	48.231	44.878	7%

Figure 36 below shows the moment/strip variation along the depth of the section.

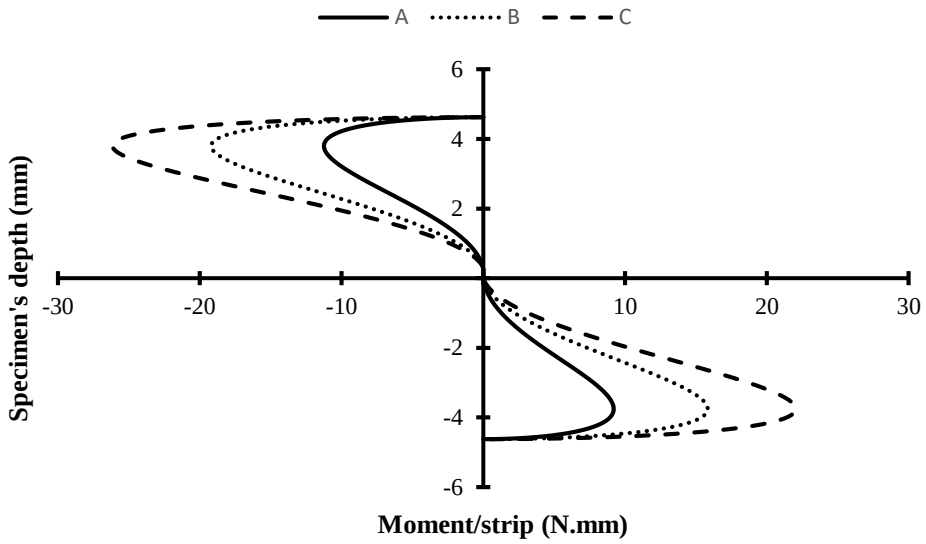

Figure 36- Moment/strip for a strip thickness of d/4000

It is observable that there is a small difference between the moment resistance and the applied moment where the difference did not exceed 10%. This error was expected as there was a difference between internal forces in the equilibrium check earlier. The small differences obtained were considered to be acceptable and likely due to the combination of experimental measurement errors and plane strain assumptions.

7. Partial Experimentation Approach

Testing GFRP bars in flexure, compression, and tension in this study made it possible to determine their mechanical properties in each loading scenario. However, testing GFRP bars in all the previously mentioned loading scenarios can be challenging and time consuming, especially given there is limited guidance for testing GFRP bars in compression, and the compression test proposed and performed in this project couldn't deliver consistently accurate results as the load applied was found to be eccentric. Moreover, testing the bars in tension until they reach failure is difficult to accomplish as gripping bars is difficult. Hence, an approach that is less time consuming and requires less testing and gives similar results is important to be found.

7.1 Required Tests

This method requires the bars to be tested in two loading scenarios only which are flexure and tension without having them to be tested in compression. In flexure, the bars should be tested according to ASTM D790 – 17 [11] which is the same standard test method used in the flexure test in this study. In this approach there is no need to use DIC, rather a strain gauge can be placed on the bottom fibres of the GFRP bar to measure tension strains. In tension, the bars should be tested according to ASTM D7205/7205M – 06 [13], the same standard test method we used in this study. For tension it may be only necessary to determine elastic modulus, not to bring the bars to failure. This means there may be no need to sand coat the anchorage lengths of the bar, and using a more affordable expansive mortar such as Betonamit may be applicable.

7.2 Analysis Procedure

The testing will result in the tensile elastic modulus, the applied moment, and the tensile strain in the FRP at the maximum moment location. Assumptions from the previous analysis including plane strain along the depth of the section and that the tensile and compressive moduli of the material is linear are used in this analysis. As observed in this study, there is a potential difference in the compressive and tensile elastic moduli meaning that the neutral axis should not necessarily be assumed to be at the section mid-height and that the stress over the height of the section is bi-linear rather than linear. Using these measurements and assumptions, the following properties are able to be determined through sectional analysis:

- The neutral axis location.
- The ultimate compressive strain on the top fibres of the bar.
- The ultimate stress in both tension and compression.
- The modulus of elasticity in compression.

For the sake of simplicity, and to make the analysis procedure for this approach more clear, consider a rectangular GFRP section that has a depth and width of **h** and **b** respectively as shown in Figure 37.

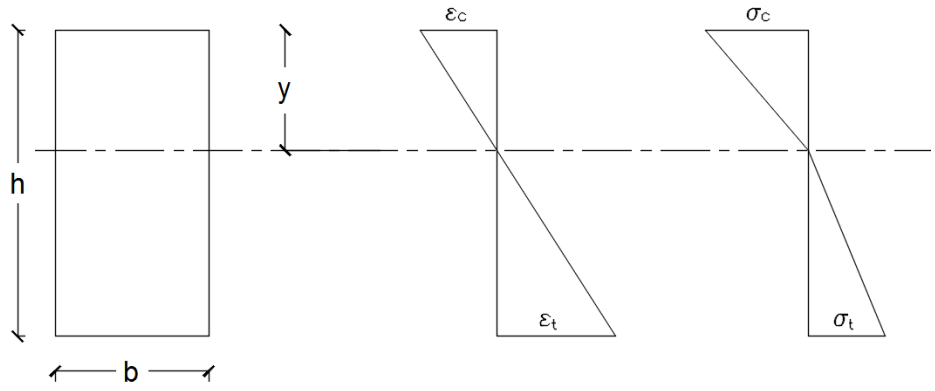

Figure 37- GFRP tensile and compressive behavior

By knowing the ultimate tensile strain on the bottom (tension) fibres of the section from the flexure test, and the tensile elastic modulus from the tension test, the ultimate tensile stress can be computed directly by multiplying the modulus by strain ($\sigma_{t,max} = E_t.\varepsilon_t$).

Using a bilinear stress assumption and satisfying force equilibrium, the total tension force and the total compression forces are computed as the volume of their corresponding stress blocks as follows:

$T= \frac{1}{2}.\sigma_t.(h–y).b$

$C= \frac{1}{2}.\sigma_c.y.b$

Where ; T= Total tension force, N

C= Total Compression force, N

h= total depth of the section, mm.

y= neutral axis depth measured from the top face,

b= width of the section, mm.

σ_t= ultimate tensile stress, MPa.

σ_c= ultimate compressive stress, MPa.

Also, from equilibrium, the internal moment resistance is equal to the applied moment. The moment resistance is computed as follows:

$M_{resistance}= T.(\frac{2}{3}y + \frac{2}{3}(h-y))$

Hence by equating the applied moment to the moment resistance, and by rearranging the equation above, the neutral axis depth can be calculated using the following formula:

$y= h - \frac{3M_a}{h.\sigma_T b}$

By knowing the neutral axis location and by assuming plane strain along the depth of the section (linear strain over the section's depth), the ultimate compressive strain on the top fibres can be computed using the following equation:

$$\varepsilon_c = \frac{\varepsilon_t . y}{h-y}$$

Where, T= Total tension force, N

C= Total Compression force, N.

h= total depth of the section, mm.

y= neutral axis depth measured from the top face, mm.

b= width of the section, mm.

M_a= applied moment, N.mm.

σ_t= ultimate tensile stress, MPa.

σ_c= ultimate compressive stress, MPa.

ε_c= ultimate compression strain, mm/mm.

ε_t= ultimate tension strain, mm/mm.

Determining the neutral axis depth makes it possible to determine the ultimate compressive stress by applying the principal of horizontal equilibrium. By applying horizontal equilibrium (T = C), the ultimate compressive stress can be computed as follows:

$$\sigma_c = \frac{\sigma_t (h-y)}{\sigma_c}$$

After calculating the ultimate compressive strain and ultimate compressive stress the compressive modulus of elasticity can be found using the following equation:

$$E_c = \frac{\sigma_c}{\varepsilon_c}$$

This example considered a rectangular section to present the approach in a simple way since the width of the section is uniform. It also shows that this approach is valid and can be applied to determine the mechanical properties of GFRP material in different shapes. However, for circular sections similar to what are included in this study, a layer-by-layer sectional analysis is required to apply this approach as the width of the section is not uniform and is changing over the depth of the section.

7.3 Partial Experimentation Approach Sectional Analysis

In this section, sectional analysis will be performed on the same specimen at the same loading stages that were performed previously to compare between the two approaches and check the validity of this approach on circular sections.

7.3.1 Experimental Data

The data that will be used in this analysis will be from the previous tests performed, however, this time only the tensile strain and the applied moment data from the flexure test along with the tensile elastic modulus (E_t = 42.237 GPa) will be used to determine material properties.

Figure 38 and Table 12 below show the moments and tensile strains at each loading stage used for this analysis.

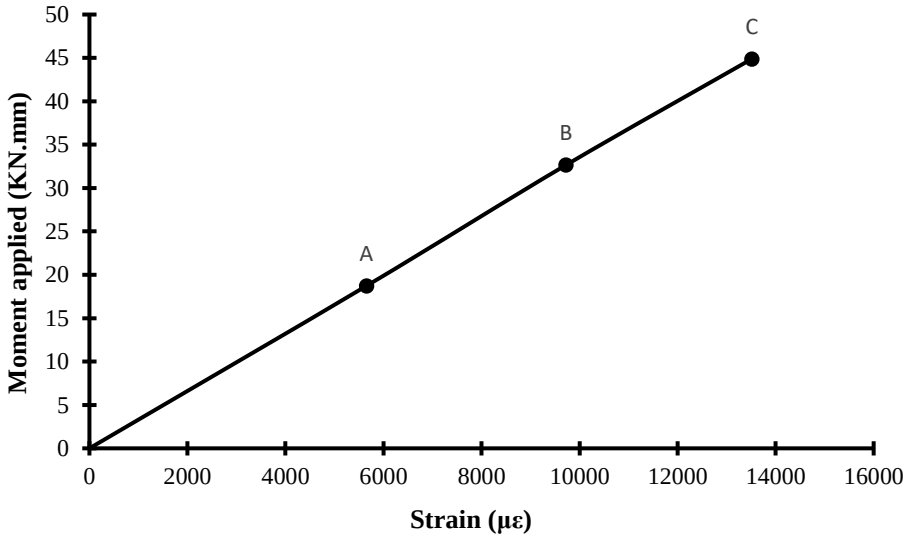

Figure 38- Flexure test experimental data at the given loading stages

Table 12- Testing data summary

Stage	ε_T (με)	$M_{applied}$ (KN.mm)	Et (MPa)
A	5652	18.724	42.237
B	9722	32.649	42.237
C	13512	44.878	42.237

7.3.2 Analysis Procedure and Results

From knowing the tensile strain on the bottom fibres, the tensile elastic modulus, and the applied moment, the following parameters were determined: the neutral axis depth, the compressive elastic modulus, the compressive strain on the top fibres, and both the tensile and compressive stresses. Only two equations were needed to find all these parameters:

1. $C - T = 0$
2. $M_r = M_a = C.d = T.d \rightarrow M_a / M_r = 1$

Where; T= Total tension force (sum of forces in all slices in tension).

C= Total compression force (sum of forces in all slices in compression).

d= Distance between tensile total and total compression forces.

M_a= Applied moment

M_r= Moment resistance

To solve this problem the values of the neutral axis depth and the compressive elastic modulus were assumed and iterated upon until both moment and force equilibrium in the section was satisfied. A spreadsheet was used for the sectional analysis, and the values of the elastic modulus "E_c" and neutral axis depth "y" were calculated using the Solver functionality (an Excel add-in) to find the values of both parameters in order to satisfy the equilibrium equations listed above that were used as constraints.

Therefore by assuming plane strain over the depth of the section, the ultimate strain in the top fibres and both tensile and compressive stresses are computed similarly to what was done in the previous sectional analysis. Table 13 below summarizes the results obtained from the sectional analysis.

Table 13- Partial experimentation approach results summary

Stage	y (mm)	E_c (GPa)	ε_c (με)	ΣF	Mr/Ma
A	4.593	43.633	5575	0.000	1.000
B	4.546	45.784	9395	0.000	1.000
C	4.584	44.033	13276	0.000	1.000

An assumption that the modulus of elasticity for the material in compression is constant over the compression range suggests that the average of the values computed at different moments should be taken for accuracy. The elastic modulus in compression was found to be 44.483 GPa. Figure 39 and Figure 40 illustrate the strain and the stress distribution over the depth of the section respectively.

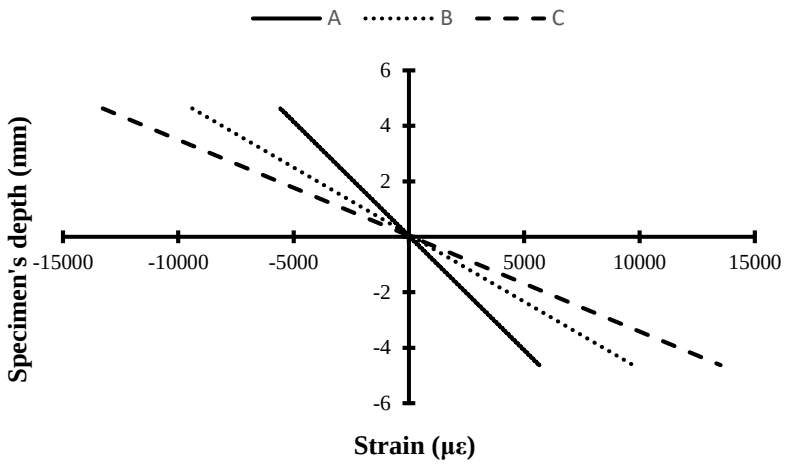

Figure 39- Strain over the section depth at the different loading stages

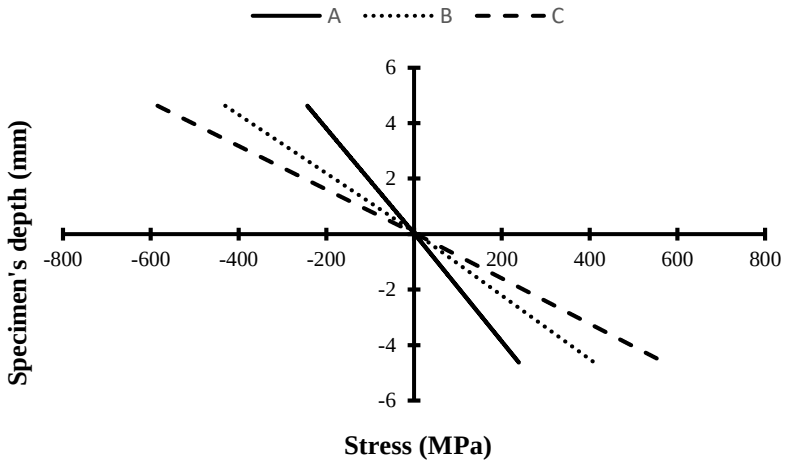

Figure 40- Stress distribution over the section depth at the different loading stages

7.3.3 Partial Experimentation vs Full Experimentation

Table 14, Table 15, and Table 16 summarize the difference between the two approaches for the neutral axis depth, the ultimate compressive strain, and the compressive elastic modulus respectively.

Table 14- Neutral axis depth difference between the two approaches

	full experimentation	**Partial experimentation**	
Stage	**y (mm)**	**y (mm)**	**% difference**
A	4.384	4.593	5%
B	4.369	4.546	4%
C	4.329	4.584	6%

Table 15- Strain difference between the two approaches

	full experimentation	**partial experimentation**	
Stage	**ε_c (με)**	**ε_c (με)**	**% difference**
A	5092.345	5574.768	9%
B	8701.575	9395.014	8%
C	11886.378	13275.782	12%

Table 16- Compressive elastic modulus between the two approaches

Full experimentation	**partial experimentation**	
E_c	**E_c**	**% difference**
58.682	44.483	24%

In some instances, the two methods resulted in substantial differences. Despite the small difference between the neutral axis depths (around 5%), and the relatively small difference in the ultimate compressive strain on the top fibres that was around 10%, the compressive elastic modulus for the partial experimentation approach was less than that of the full experimentation by 24%.Moreover, the reduction in the elastic modulus is the reason why the stress was not bilinear in Figure 40 as expected from the previous analysis.

The reason behind the large difference in the compressive elastic modulus could be due to the small cross-section of the tested bars, and if the test was performed on a larger bar diameter, 20 mm diameter or larger, the difference could have been less.

Based on these results, it is advised to perform the partial experimentation approach with a specimen that has a larger diameter to check and confirm its validity.

8. Conclusion

The purpose of this project was to experimentally study and report the behavior of GFRP bars, and determine their mechanical properties in flexure, compression, and tension. The conclusions of this experimental study are as follows:

Testing GFRP bars in flexure according to ASTM D790 – 17 [11] was successful as it delivered the results and type of failure that was expected. All the specimens failed abruptly by compression at the location of the top fibres. The test method is an appropriate test method to study the flexural behavior of GFRP bars and can be adopted to test different sizes of bars.

On the other hand, ASTM D7205/7205M – 06 [13] needs to be modified to test GFRP bars in tension in order to reach failure. The standard test method does not mention anything about sand coating the anchorage lengths, which helps in increasing the friction between the bar and the expansive mortar inside the anchors to keep the bar firmly attached to it, allowing the test to progress until failure occurs which is characterized in the splitting of fibres of the bar's free length.

Although the results obtained from the compression test proposed were assumed to be valid, the test still needs to be adjusted such that it ensures the loading of the specimen to be concentric, in order to avoid the small errors observed. Concentric loading will result in having a uniform strain over the depth of the specimen which will ensure correct strain values and elastic modulus values may be measured without the use of DIC.

The ultimate tensile and compressive strengths the 9.25 mm GFRP bars reached from the tests performed were 944 MPa and 252 MPa respectively. The elastic modulus in compression was found to be larger than that in tension by approximately 33%, as the tensile elastic modulus average was 42.237 GPa and that in compression was 58.682 GPa. The difference in the elastic moduli contradicts with what Khan et al. [5] obtained in their study, where, they found that the tensile elastic modulus was larger than the compressive elastic modulus. The difference in the elastic moduli results is due to the modification that Khan et al. [12] made on ASTM D695 – 15 [12] to try making it suitable to test GFRP bars in compression. However, modifying ASTM D695 – 15 [12] would not yield valid results as it was not made specific to test GFRP bars in compression which makes the compressive data they obtained from testing unreliable.

The neutral axis depth was found to be shifted upwards away from the center towards the top fibres of the bar that are undergoing compression which was due to the difference between the tensile and compressive elastic moduli. Additionally, it was found from the flexure test that the strains over the depth of the section proves that the Euler-Bernoulli theorem of having a plane strain is applicable. The horizontal equilibrium was satisfied from the beginning of loading until failure, and the moment resistance was always equal to the applied moment, disregarding the small difference due to some small experimental errors.

The partial experimentation approach requires flexure tests with strain monitoring in the extreme bottom fibre, and tension tests to determine the tensile elastic modulus. Applying equilibrium in both internal force and internal moment will result in computed values of compression properties including ultimate strain (for compression dominate failure) and

elastic modulus. However, this procedure was found to give a substantial difference in the compressive elastic modulus compared to what was obtained when considering the results from the three tests performed (compression, tension and flexure) independently. This large difference may be due to the small diameter of the bar that was tested in flexure resulting in measurement and calculation errors.

The importance of having a standard test method to test GFRP bars in compression was evident in the results obtained from the partial experimentation approach. The results obtained proved that the compressive elastic modulus obtained from analyzing the tensile and flexural data would not yield results that represent the actual compressive elastic modulus of GFRP.

Therefore, more research should be done on determining the compressive properties of GFRP bars, through designing a purely axial standard test method for testing GFRP bars in compression, which ensures concentric loading of the bars, and yield accurate and reliable data.

References

[1] Landesmann, A., Seruti, C.A, & Batista, E.M. Mechanical Properties of Glass Fiber Reinforced Polymers Members for Structural Applications. Materials Research, 18(6). (2015). (p.p. 1372-1383). https://dx.doi.org/10.1590/1516-1439.044615.

[2] T. (n.d.). Advantages of Using Glass Fiber Reinforced Polymer (GFRP) Rebar. Retrieved from https://www.tuf-bar.com/advantages-of-using-glass-fiber-reinforced-polymer-gfrp-rebar/.

[3] Dutton, M., "Digital image correlation for evaluating structural engineering materials*"*. (2012). Master's thesis. Queen's University, Kingston, Ontario, Canada.

[4] McEnteggart, I., *"*An introduction to digital image correlation*"*. (2012). www.instron.us/en-us/our-company/press-room/blog/2015/august/dic-slideshare

[5] Khan, Q. S., Sheikh, M.N., & Hadi, M. N. S, *"*Tension and compression testing of fibre reinforced polymer (FRP) bars*"*, In Z. Wu, G. Wu & X. Wang (Eds.), Joint Conference of the 12th International Symposium on Fiber Reinforced Polymers for Reinforced Concrete Structures (FRPRCS-12) & the 5th Asia-Pacific Conference on Fiber Reinforced Polymers in Structures (APFIS-2015). (2015). (pp. 1-6).

[6] Khorramian, K., & Sadeghian, P., "New testing method of GFRP bars in compression*"*, Dalhousie University. (2018). Canadian Society for Civil Engineering 2018 Conference.

[7] Benmokrane, B., Zhang, B., & Chennouf, A, *"*Tensile properties and pullout behaviour of AFRP and CFRP rods for grouted anchor applications*",* Construction and Building Materials, 14(3). (2000). (p.p. 157-170).

[8] Kocaoz, S., Samaranayake, V., & Nanni, A, *"*Tensile characterization of glass FRP bars*"*, Composites Part B: Engineering, *36*(2). (2005). (p.p. 127-134), doi:10.1016/j.compositesb.2004.05.004.

[9] Gudonis, E.; Timinskas, E.; Gribniak, V.; Kaklauskas, G.; Arnautov, A. K.; Tamulėnas, V. FRP reinforcement for concrete structures: state-of-the-art review of application and design, Engineering Structures and Technologies 5(4). (2013). (p.p. 147–158). http://dx.doi.org/10.3846/2029882X.2014.

[10] Bowlby, L., "Evaluating the potential of high SSA biochar particles produced via microwave pyrolysis as reinforcing filler in pultruded fiber-reinforced polymer composites". (2018). Master's thesis. University of New Brunswick.

[11] ASTM Standard D790-17, "Standard Test Methods for Flexural Properties of Unreinforced and Reinforced Plastics and Electrical Insulating Materials", ASTM international, West Conshohocken, PA. (2017). DOI: 10.1520/ D0790-17, https://www.astm.org/Standards/D790.htm.

[12] ASTM Standard D695-15, *"*Standard Test Method for Compressive Properties of Rigid Plastics*",* ASTM international, West Conshohocken, PA. (2015). DOI: 10.1520/D0695-15, https://www.astm.org/Standards/D695.htm.

[13] ASTM Standard D7205/7205M-06, "Standard Test Method for Tensile Properties of Fiber Reinforced Polymer Matrix Composite Bars", ASTM international, West Conshohocken, PA. (2016). DOI: 10.1520/D7205_D7205M-06R16, https://www.astm.org/Standards/D7205.htm

[14] ASTM Standard D3916 - 08, "Standard Test Method for Tensile Properties of Pultruded Glass-Fiber-Reinforced Plastic Rod", ASTM international, West Conshohocken, PA. (2016). DOI: 10.1520/D3916-08R16. https://www.astm.org/Standards/D7205.htm

Appendix

Figure 41 - Figure 45 show the tensile and compressive strain variation with respect to time for the extreme bottom and top fibres respectively for all specimens tested in flexure at the location of maximum moment (midspan).

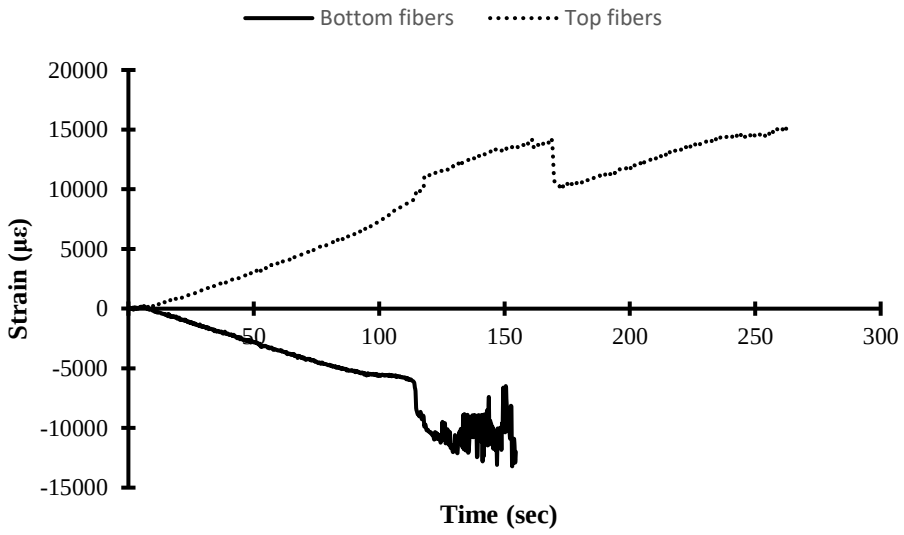

Figure 41- Specimen F1 tensile and compressive strains with respect to time

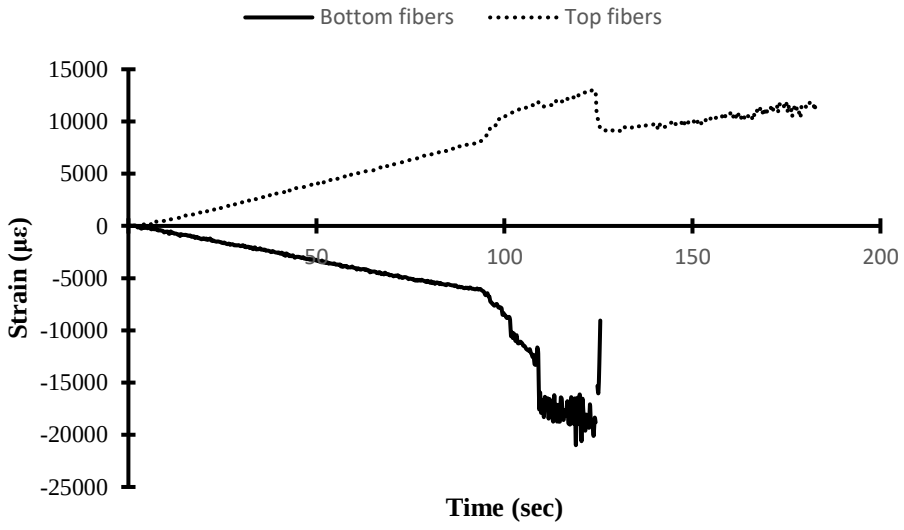

Figure 42- Specimen F2 tensile and compressive strains with respect to time

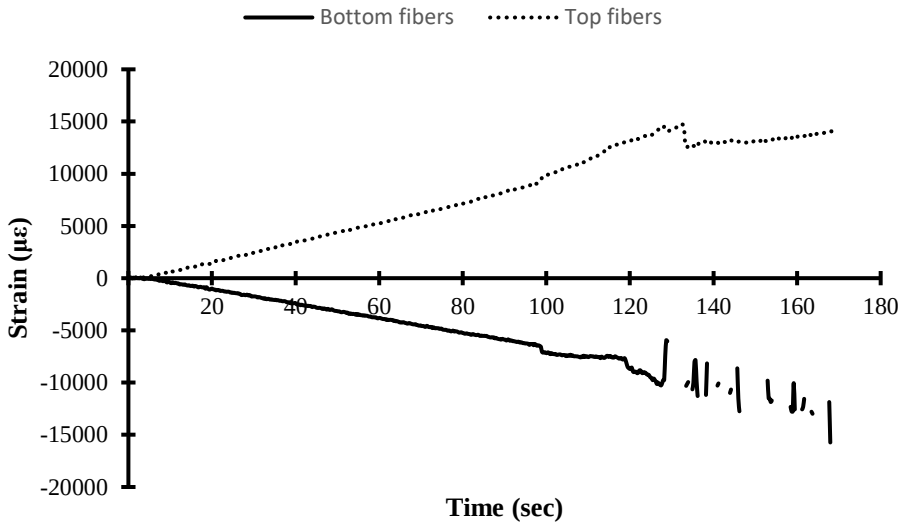

Figure 43- Specimen F3 tensile and compressive strains with respect to time

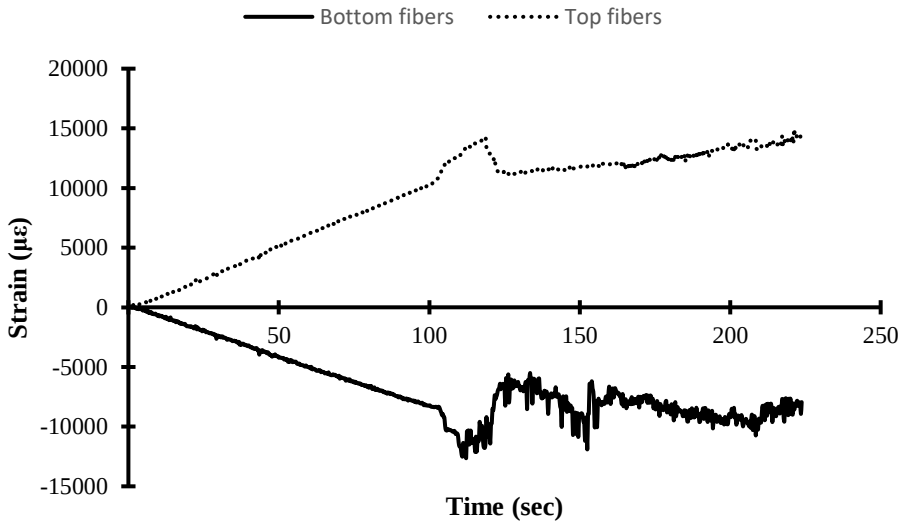

Figure 44- Specimen F4 tensile and compressive strains with respect to time

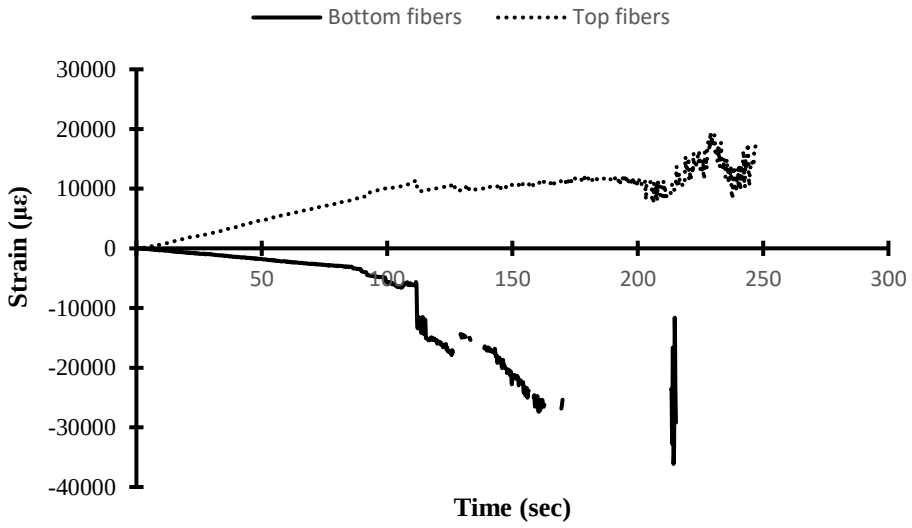

Figure 45- Specimen F5 tensile and compressive strains with respect to time

Figure 46 and Figure 47 show the force/strip and moment/strip variation along the depth of the section respectively for the partial experimentation approach (partial experimentation approach is the approach that required testing the bars in flexure until failure, and in tension to obtain the tensile elastic modulus only without having the necessity of achieving failure).

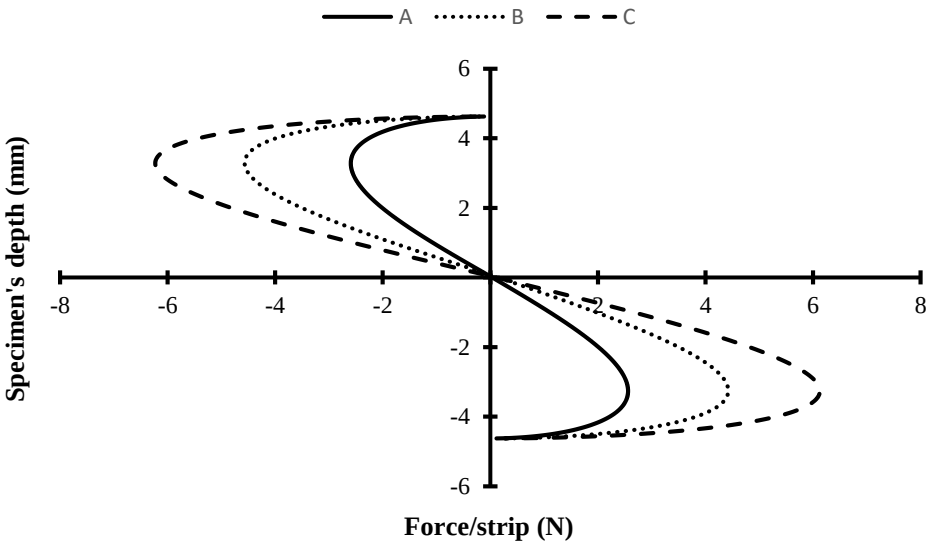

Figure 46- Partial experimentation approach force/strip - strip thickness of d/4000

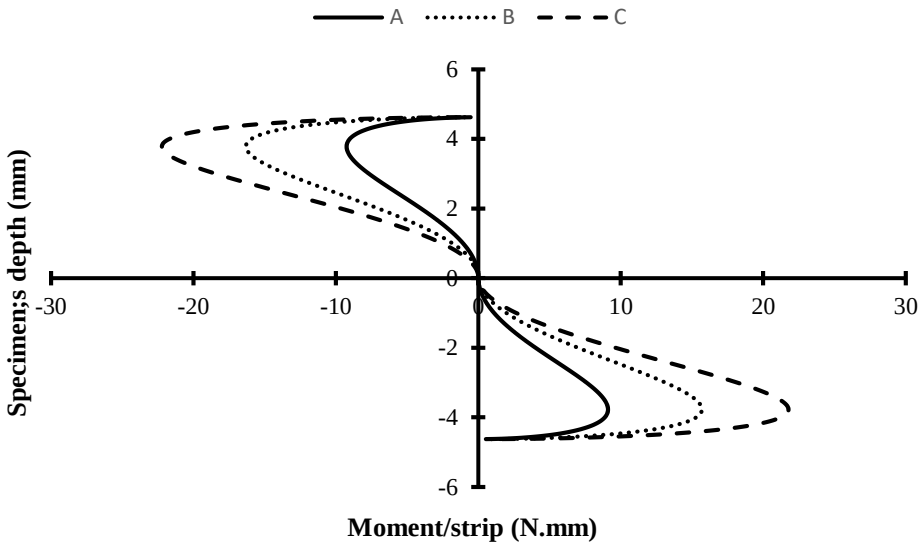

Figure 47- Partial experimentation approach moment/strip - strip thickness of d/4000

Curriculum Vitae

Candidate’s full name: Mahmoud Saleh Abou Niaj.

Universities attended: Beirut Arab University.

Degree: Bachelor of Science in Civil and Environmental Engineering.

Place: Beirut, Lebanon.

Date: June, 2016.